UNIVERSITY OF HAWAI'I LIBRARY

A334

SEMI-ACTIVE CONTROL OF BUILDING STRUCTURES USING MR DAMPERS BASED ON A MODIFIED INVERSE DYNAMIC MODEL

A THESIS SUBMITTED TO THE GRADUATE DIVISION OF THE

UNIVERISTY OF HAWAI'I IN PARTIAL FULFILLMENT

OF THE REQUIREMENTS FOR THE DEGREE OF

MASTER OF SCIENCE

IN

CIVIL ENGINEERING

AUGUST 2008

By

Xiaochuan Yu

Thesis Committee:

Tianwei (David) Ma, Chairperson

H. Ronald Riggs

Si-Hwan Park

We certify that we have read this thesis and that, in our opinion, it is satisfactory in scope and quality as a thesis for the degree of Master of Science in Civil Engineering.

THESIS COMMITTEE

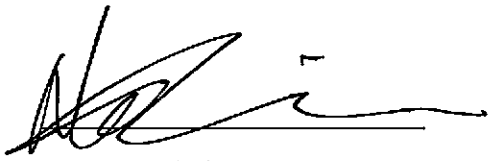

Chairperson

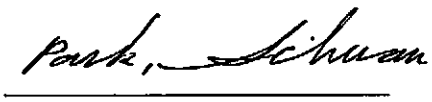

ACKNOWLEDGEMENTS

Great thanks to my family, my friends, and my colleagues in Hawaii. Special thanks to the members of the thesis committee for their continued guidance and support.

ABSTRACT

This thesis presents a new semi-active strategy to adjust the voltage of a magnetorheological (MR) damper to track the optimal/desired damper force by the Linear Quadratic Regulator (LQR) method. Integrated with the new strategy, a modified inverse dynamic model is proposed to evaluate the value of evolutionary variable z.

The new strategy is applied to numerical examples including one-story buildings with different periods (stiff, moderate and flexible). White Gaussian noise (WGN) and 1940 El Centro earthquake are chosen as excitations. The numerical results indicate that this new strategy is effective and practically implementable in reducing the structural responses under various excitations. Furthermore, its effectiveness in structural control of buildings is compared with passive-on and passive-off cases. In addition, various factors that influence the MR damper's performance, including control force weighting coefficient R, periods of buildings, types of excitation and its amplitude, are presented and discussed. And an appropriate way to choose R is also recommended. Finally, this strategy is numerically applied to a six-story building model. The results show that the MR damper also performs well in vibration control of multi-story buildings.

CHAPTER 1 INTRODUCTION **1**

1.1 Background 1

1.2 Types of Semi-active Devices 2

1.3 MR Fluids 6

1.4 Applications of MR technologies in Civil Engineering 9

1.5 Problem statement 11

CHAPTER 2 MODELS OF MR DAMPER **13**

2.1 Various Models of MR Damper 13

2.2 Bouc-Wen Model 14

2.3 Some Properties of Bouc-Wen Model 16

2.4 Semi-active Control Algorithms 17

2.4.1 Lyapunov Controller Algorithm 19

2.4.2 Clipped-optimal Controller 20

2.4.3 Fuzzy Logic Controller 22

CHAPTER 3 CONTROL METHOD AND TRACKING STRATEGIES **24**

3.1 State-Space Model 24

3.2 Optimal Control Method 24

3.2.1 Continuous Linear Quadratic Regulator (LQR) 24

3.2.2 Software Implementation of the LQ Regulator 26

3.3 Two Different Tracking Strategies 27

3.3.1 Based on a Modified Inverse Dynamic Model 28

3.3.2 Direct Method 30

CHAPTER 4 CASE STUDY 33

4.1 Uncontrolled Case and Controlled Cases 33

4.2 Case Study: One-story Building 34

4.2.1 Validation of the New Control Strategy 35

4.2.2 Stiff One-story Building Excited by WGN 39

4.2.3 Moderate and Flexible One-story Buildings Excited by WGN 43

4.2.4 Stiff One-story Building Excited by 1940 El-Centro Earthquake 49

4.2.5 Moderate and Flexible One-story Buildings Excited by 1940 El-Centro Earthquake 53

4.3 Case Study: Six-story Building 59

4.4 Introduction of Program 62

CHAPTER 5 CONCLUSIONS AND FUTURE WORK 64

5.1 Conclusions 64

5.2 Future Work 65

REFERENCE 66

APPENDIX 72

LIST OF TABLES

Table Page

4.1. Properties of different one-story buildings……..…..34

4.2. Reduction ratios of responses at passive-cases (excited by WGN)……..43

LIST OF FIGURES

Figure Page

1.1 Schematic diagram and model of the SASD....4

1.2 Analytical model of the variable device (SAIVD & SAIVF)....5

1.3 Shear strength versus shear strain rate for the Bingham plastic material model.7

1.4 Typical shear stress versus strain curves for MR fluid.... ...8

1.5 Semi-active control system for a structure integrated with an MR damper.....12

2.1 Binham model of controllable damper....13

2.2 Extended Binham model....13

2.3 BingMax model.... 14

2.4 Viscoelastic plastic model....14

2.5 Simple Bouc-Wen model.... 15

2.6 Modified Bouc-Wen model....15

2.7 Graphical view of clipped-optimal control.... ...21

3.1 Continuous LQ regulator simulation procedure....27

3.2 Comparison of displacements of stiff one-story building using one MR damper.... ..31

3.3 Comparison of $x-z$ relationship....32

4.1 Displacement of stiff one-story building at uncontrolled and controlled cases, excited by El-Centro earthquake....36

4.2 Absolute acceleration of stiff one-story building at uncontrolled and controlled cases, excited by El-Centro earthquake....36

4.3 Evolutionary variable z versus displacement x 37

4.4 Time history of the commanding voltage....38

4.5 Comparison of the desired damping force and the actual damping force....38

Figure Page

4.6 Peak displacement of stiff one-story building excited by different amplitudes of WGN, compared with results derived from LQR method.....40

4.7 RMS displacement of stiff one-story building excited by different amplitudes of WGN.....40

4.8 Peak acceleration of stiff one-story building excited by different amplitudes of WGN.....41

4.9 RMS acceleration of stiff one-story building excited by different amplitudes of WGN.....41

4.10 Percentage of voltages between minimum and maximum for stiff one-story building excited by different amplitudes of WGN.....42

4.11 Peak displacement of moderate one-story building excited by different amplitudes of WGN.....44

4.12 RMS displacement of moderate one-story building excited by different amplitudes of WGN.....45

4.13 Peak acceleration of moderate one-story building excited by different amplitudes of WGN.....45

4.14 RMS acceleration of moderate one-story building excited by different amplitudes of WGN1.....46

4.15 Percentage of voltages between minimum and maximum for moderate one-story building excited by different amplitudes of WGN 46

4.16 Peak displacement of flexible one-story building excited by different amplitudes of WGN.....47

4.17 RMS displacement of flexible one-story building excited by different amplitudes of WGN.....47

4.18 Peak acceleration of flexible one-story building excited by different amplitudes of WGN.....48

4.19 RMS acceleration of flexible one-story building excited by different amplitudes of WGN.....48

Figure Page

4.20 Percentage of voltages between minimum and maximum for flexible one-story building excited by different amplitudes of WGN.....49
4.21 Peak displacement of stiff one-story building excited by different amplitudes of El-Centro earthquake.....50
4.22 RMS displacement of stiff one-story building excited by different amplitudes of El-Centro earthquake.....51
4.23 Peak acceleration of stiff one-story building excited by different amplitudes of El-Centro earthquake.....51
4.24 RMS acceleration of stiff one-story building excited by different amplitudes of El-Centro earthquake.....52
4.25 Percentage of voltages between minimum and maximum for stiff one-story building excited by different amplitudes of El-Centro earthquake.....52
4.26 Peak displacement of moderate one-story building excited by different amplitudes of El-Centro earthquake.....54
4.27 RMS displacement of moderate one-story building excited by different amplitudes of El-Centro earthquake.....54
4.28 Peak acceleration of moderate one-story building excited by different amplitudes of El-Centro earthquake.....55
4.29 RMS acceleration of moderate one-story building excited by different amplitudes of El-Centro earthquake.....55
4.30 Percentage of voltages between minimum and maximum for moderate one-story building excited by different amplitudes of El-Centro earthquake.....56
4.31 Peak displacement of flexible one-story building excited by different amplitudes of El-Centro earthquake.....56
4.32 RMS displacement of flexible one-story building excited by different amplitudes of El-Centro earthquake.....57
4.33 Peak acceleration of flexible one-story building excited by different amplitudes of El-Centro earthquake.....57

Figure Page

4.34 RMS acceleration of flexible one-story building excited by different amplitudes of El-Centro earthquake.....58

4.35 Percentage of voltages between minimum and maximum for flexible one-story building excited by different amplitudes of El-Centro earthquake.....58

4.36 Schematic view of the six-story building model with one MR damper.....59

4.37 Peak displacement of the 1st floor of six-story building excited by different amplitudes of El-Centro earthquake.....60

4.38 RMS displacement of the 1st floor of six-story building excited by different amplitudes of El-Centro earthquake 60

4.39 Peak acceleration of the 1st floor of six-story building excited by different amplitudes of El-Centro earthquake.....61

4.40 RMS acceleration of the 1st floor of six-story building excited by different amplitudes of El-Centro earthquake.....61

4.41 Percentage of voltages between minimum and maximum for the 1st floor of six-story building excited by different amplitudes of El-Centro earthquake...62

4.42 Flowchart for program.....63

4.43 Flowchart for module "CONTROL".....63

CHAPTER 1 Introduction

1.1 Background

Since the initial conceptual study by Yao in 1972, the evolution of structural control in civil engineering has been rapid, attracting the interest and attention of numerous researchers in the past decades. Researchers classify the control systems as passive, active, hybrid and semi-active control systems (Soong 1990; Housner et al. 1997; Spencer 2003; Chu et al. 2005).

(1) Passive damping strategies, including base isolation systems, viscoelastic dampers and tuned mass dampers, are well understood and are widely accepted by industry. However, these passive devices are unable to adapt to structural changes and to varying usage patterns and loading conditions (Spencer 2003).

(2) The hybrid control generally refers to a combined passive and active control system. A portion of the control objective is accomplished by the passive system, implying that less power and resources are required in a properly designed hybrid system.

(3) Active control systems apply forces to the structure in a prescribed manner. In an active feedback control system, the signals sent to the control actuators are a function of the response of the system measured with physical sensors (optimal, mechanical, electrical, chemical and so on.)

(4) Semi-active control devices are often viewed as controllable passive devices, yet maintaining versatility and adaptability of fully active systems and requiring no

large external energy. In contrast to active control devices, semi-active control devices do not have the potential to destabilize the structural systems.

1.2 Types of Semi-active Devices

Semi-active control systems, which have been proposed and investigated in the literature (He W.L. et al., 2003), include active variable dampers (AVD), active variable stiffness systems (AVS), electrorheological (ER) dampers, magnetorheological (MR) dampers, continuous variable stiffness dampers, semi-active friction dampers. Various active control theories have been used and compared by researchers.

Spencer and Nagarajaiah (2003) classified the semi-active control systems as variable-orifice fluid dampers, variable-stiffness devices, controllable friction devices, smart tuned mass dampers and tuned liquid dampers, controllable fluid dampers and controllable dampers.

(1) Variable-orifice dampers

Feng and Shinozuka (1990) applied this type of variable-damping device to control the motion of bridges experiencing seismic motion. Patten and Sack (1996) retrofitted an existing bridge using a semi-active hydraulic bridge vibration absorber, and an experimental test of the new system indicated 65%-70% reduction of peak amplitude. Spencer and Nagarajaiah (2003) summarized that approximately 800 semi-active variable-orifice fluid dampers have been installed in building structures in Japan.

Wongprasert and Symans (2005) experimentally evaluated the seismic response of a scale-model, base isolated, three-story building frame, using low-damping rubber (LDR) bearings along with semi-active variable-orifice fluid dampers to provide adaptive damping to the isolation system. Yang et al. (1995) numerically studied its application for bridge structures.

(2) Variable-stiffness Device

Kobori et al. (1993) implemented a full-scale variable-orifice damper, using on-off mode, in a semi-active variable-stiffness system to investigate semi-active control of the Kajima Research Institute building. Yang et al. (1996) studied the control of seismic excited buildings using active variable stiffness systems.

Nagarajaiah and Mate (1998) developed a semi-active continuously and independently variable-stiffness device (SAIVS). This device can vary the stiffness continuously and smoothly to effectively control the vibration and produce a non-resonant system. A new control algorithm for SAIVS device was developed and implemented in shake table tests (Sahasrabudhe and Nagarajaiah, 2005), and it reduced bearing displacements further than the passive cases, while maintaining forces at the same level as the minimum stiffness case.

Djajakesukma et al. (2002) presented study of a semi-active stiffness damper (SASD) in a five-story model against earthquake loads, with its schematic diagram given in Fig. 1.1.

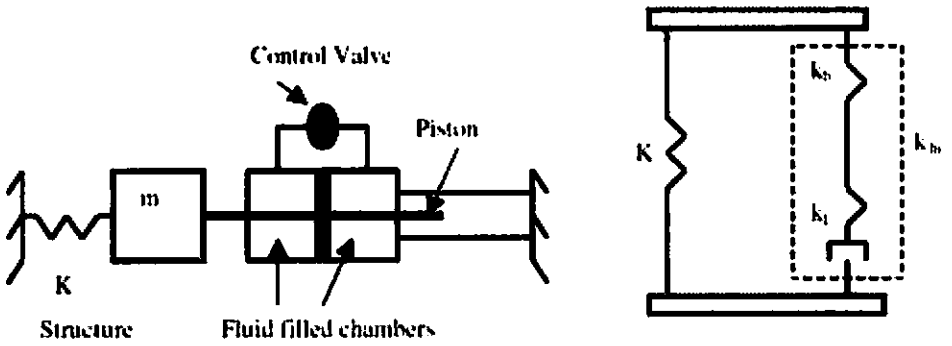

Fig. 1.1 Schematic diagram and model of the SASD

(3) Smart tuned mass dampers

Tuned mass dampers (TMDs) have been utilized in wind vibration control and seismic control of buildings with various levels of success. Smart tuned mass dampers (STMD) with adjustable damping, first studied by Hrovat et al. (1983), offers additional advantages over TMDs. STMDs have been used for vibration reduction of mechanical and civil engineering structures.

STMDs can also be based on controllable tuned sloshing dampers (CTSD) (Lou et al. 1994) and controllable tuned liquid column dampers (CTLCD) (Yalla et al. 2001).

(5) Variable friction dampers

Various semi-active devices have been proposed which utilize force generated by surface friction to dissipate vibratory energy in a structural system (Akbay and Aktan 1991; Kannan et al. 1995; Feng et al. 1993). A variable damping element (VDE) can control a reactive internal force within its capacity range, and numerous studies on VDE can be found in the "*Proceedings of Japan National Symposium on Structural Response Control, Tokyo, 1992*".

Recently, variable friction systems were studied by Yang and Agrawal (2002) for

seismic response reduction of nonlinear buildings. Garrett et al. (2001) studied piezoelectric friction dampers experimentally. He et al. (2003) investigated the effectiveness of smart semi-active friction dampers (SAFD) for building structures against near-field and far-field earthquakes.

Nagarajaiah and Narasimhan (2006) further developed a new semi-active variable damper (SAIVD), and it has been shown to be effective in achieving response reductions in smart base isolated buildings in near fault earthquakes. Narasimhan and Nagarajaiah (2006) developed a new variable friction device (SAIVF), which consists of four friction elements and four restoring spring elements arranged in a rhombus configuration with each arm consisting of a friction-stiffness pair. This device has achieved response reduction in smart base isolation buildings in near-fault earthquakes. Schematic view of SAIVD and SAIVF is shown in Fig. 1.2.

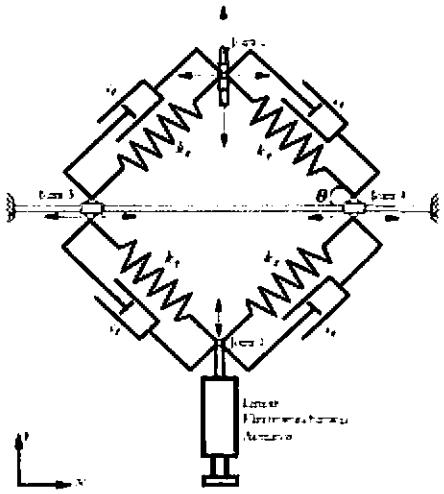

Fig. 1.2 Analytical model of the variable device (SAIVD & SAIVF)

Because semi-active control devices are intrinsically nonlinear, it is challenging to develop practical control strategies. However, various control strategies have been developed to take advantages of the particular characteristics of the semi-active

devices, including bang-bang control, clipped optimal model, bistate control, fuzzy control methods, and adaptive nonlinear control.

System integration research is another important area. Structural systems are complex combinations of individual structural components. Only integrated with efficient control strategies, the performances of semi-active devices can be enhanced. Therefore, once the advantages of semi-active control systems are fully achieved and recognized in prototype tests, a primary task for the future is to establish standards or specifications complementary to existing standards.

1.3 MR Fluids

Jacob Rabinow (1948) initially discovered magnetorheological (MR) fluids and described several potential applications. This work was almost concurrent with Winslow's electrorheological (ER) fluid work (1949). The research about MR fluids seemed stagnant for decades till its commercial application in 1990s. Weiss and Carlson (1993) provided a summary of electrorheological (ER) material research and development. Later, Weiss et al (1994) compared the yield behavior measured for ER fluid and MR fluid and presented the initial characterization of the pre-yield properties exited by MR fluid. The reheological and magnetic properties of several commercial MR fluids were further presented and discussed by Jolly et al (1999).

It should be noted that LORD Corporation and researchers worldwide largely contributed to the commercialized application of MR fluid. A more detailed review of the state of the art in MR fluid technology can be referred to this paper (Goncalves et

al. 2006).

Both MR and ER fluids exhibit remarkable field-induced change in response to an applied magnetic or electric field. Although applications details differ because of the requirements of generating strong magnetic fields, the basic physics describing how MR and ER material properties change, and the design of mechanical devices to capitalize on these changes, is similar.

When applied a magnetic field, the micron-sized ferrous particles suspended in the fluid begin to align parallel to the flux path, creating particle chains, which resist and restrict fluid movement. As a result, a field-dependent yield stress develops in the fluids, increasing as the applied field increases. In the absence of this magnetic field, MR fluid exhibits Newtonian-like behavior. Thus a Bingham plastic model can be used to simulate its property:

$\tau = \tau_y(F) + \eta\dot{\gamma}, \tau > \tau_y$ at stresses τ above τ_y

$\tau = G\gamma, \tau < \tau_y$ at stresses τ less than τ_y (1.1)

where $\tau_y(F)$ = field dependent yield stress, F = the strength of the magnetic field, G = the complex material modulus, γ = shear strain, $\dot{\gamma}$ = strain rate, η = viscosity. The response predicted by this model is plotted in Fig. 1.3.

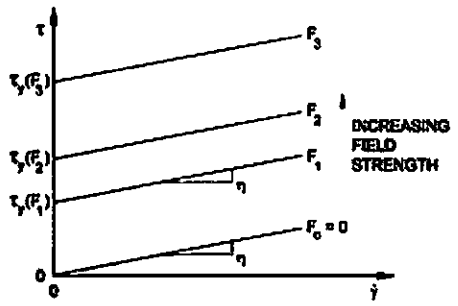

Fig. 1.3 Shear strength versus shear strain rate for the Bingham plastic material model

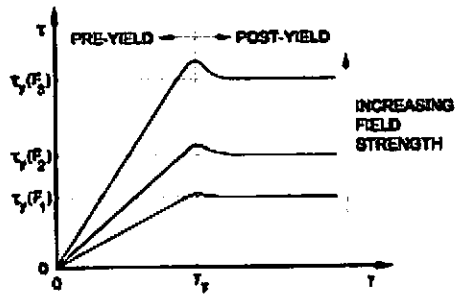

Fig.1.4 Typical shear stress versus strain curves for MR fluid

In the "Post-Yield" regime, MR fluids typically exhibit viscous properties. A static yield stress corresponds to the actual force necessary to initiate flow, while a dynamic yield stress and the plastic viscosity reflect the flow characteristics of MR fluids. In the "Pre-Yield" regime, MR fluids typically exhibit elastic properties. The transition from elastic to viscous is also defined by a yield or critical strain, in addition to the previously described static yield stress. Fig. 1.4 shows typical stress-strain characteristics for the ER or MR fluid within and beyond yield. Several parameters can be utilized to define the properties of MR fluid.

- Critical or Yield Strain ($\gamma_{critical}$)

The strain level where a material begins to transit from elastic to viscous behavior is typically defined as the yield or critical strain. Since the shear modulus of a material measured in the elastic region is only a function of temperature and frequency, the critical strain represents the strain level at which the shear modulus deviates from linear behavior.

- Storage Modulus (G') and Loss Modulus (G'')

Storage modulus (G') measures the material's ability to elastically store strain

energy, and it has been demonstrated to increase with an elevation in the applied electric field strength or frequency. Loss modulus ($G^{"}$) is associated with the dissipation of energy during deformation and can be determined by measuring the phase difference between a strain wave input to a material and the resulting stress wave (Weiss et al. 1994).

- Loss Factor ($\tan\delta$)

  Ratio of the loss modulus to the storage modulus: $G^{"}/G^{'}$.

- Yield Stress (τ_{static})

The static yield stress has previously been defined as the force necessary to initiate flow within the material. In other words, the static yield stress exhibited by a material reflects the yield point of the material. In a conventional stress versus strain plot, coordinates that reflect the static yield stress and the critical strain represent this yield point.

1.4 Applications of MR technologies in Civil Engineering

Today a number of MR fluids and MR fluid devices are commercially available. At present, MR dampers are being used for control of vibrations in automobiles, for minimizing damage to civil engineering structures due to seismic motions, for varying the stiffness of exercise equipment, and for reducing vibrations in truck seats (Jolly et al. 1999).

- Heavy Duty Vehicle Seat Suspensions: this commercial linear MR damper has served as a test bed to demonstrate that MR dampers can have long cycle lives

with no significant abrasive wear caused by the MR fluid.

- Seal-less vibration damper: the damper functions by moving a small steel disk or baffle in a chamber of MR fluid. Primary controlled motion is axial although secondary lateral and flexing motions may also be accommodated. Damping force of 0 to ±125N is produced in the primary direction. This damper may also be used as a locking device. This damper does not require dynamic, sliding seals. The relatively small amplitudes encountered (±3mm) allow the use of electrometric rubber elements instead.

Song et al. (2005, 2007) applied an MR damper in seat suspension that was used for laboratory testing. The dynamic issues inherent with the binary-like skyhook control policy were discussed. And an adaptive control strategy was applied to this suspension system and showed the effectiveness of the model-based adaptive control algorithm. MagneRide, one of the significant commercial applications in vehicle suspension systems, has been jointly developed by Delphi and Lord Corporation and was becoming standard equipment for GM luxury Cadillac cars and being pushed into Buick, too (Song 2007).

Especially in civil engineering, MR dampers have been demonstrated effective in structural control by previous lab tests (Dyke et al. 1996; Spencer et al. 1997; Yi et al. 2001). Yang et al. (2002, 2004) performed a full-scale test of a 20-ton MR damper. Dynamic response time is an important characteristic for determining the performance of MR dampers in practical civil engineering applications.

MR dampers were applied to control the 20-story seismically excited benchmark

structure (Ohtori et al. 2004; Yoshida and Dyke 2004). Yoshida and Dyke (2005) further studied the capabilities of semi-active control systems using MR dampers when applied to numerical models of full-scale asymmetric buildings.

In addition, several full-scale or half-scale tests have been performed in Taiwan, China (Loh et al. 2003; Lin et al. 2006; Loh et al. 2007), and a wireless control system was illustrated and applied into test of a full-scale structure controlled by a network of wireless sensors integrated with a semi-active MR damper (Loh et al. 2007; Lynch et al. 2007).

1.5 Problem statement

As currently researcher can only command MR damper "On" or "Off" (Jansen and Dyke 2000; Yi et al. 2001) based on clipped-optimal controller, the current research focuses on developing a new semi-active strategy for the MR damper, illustrated in Fig. 1.5, in order to command the MR damper an intermediate voltage.

A modified inverse dynamic model is proposed to adjust the voltage u_{i+1} at time $t(i+1)$ to track the optimal/desired damper force f_{ci} at $t(i)$, which is compared with damper force f_i at $t(i)$. The predicted damper force f_{i+1} at $t(i+1)$ can be obtained using Bouc-Wen model after the voltage u_{i+1} has been determined. Linear quadratic regulator (LQR) method is employed to obtain the desired/optimal damper forces.

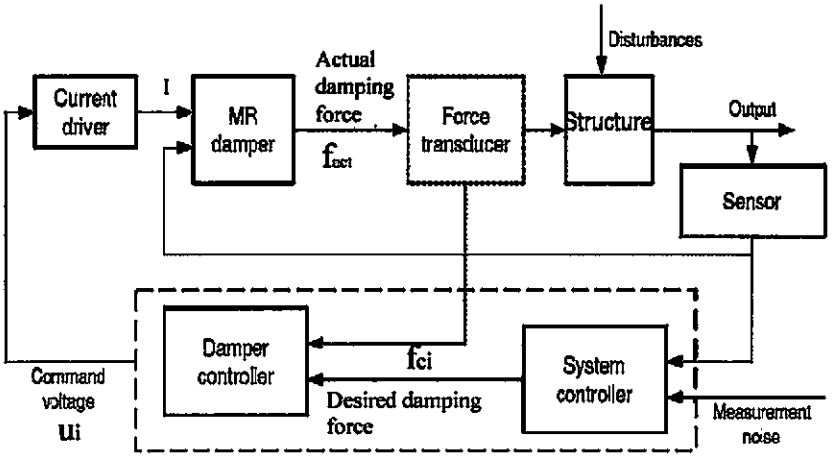

Fig. 1.5 Semi-active control system for a structure integrated with an MR damper

The first numerical example is about three one-story buildings with different periods (stiff, moderate and flexible). White Gaussian noise (WGN) in different amplitudes and 1940 El Centro earthquake are chosen as excitation. This new strategy is integrated in the above semi-active control system to control the structural responses under various excitations. Its effectiveness in structural control of buildings is compared with passive-on and passive-off cases. In addition, various factors that influence the MR damper's performance, including control force weighting coefficient R, periods of buildings, types of excitation and its amplitude, are presented and discussed. Finally, the new strategy is applied to the vibration control of a six-story building.

CHAPTER 2 Models of MR Damper

2.1 Various Models of MR Damper

Generally, there exist two general methods to model an ER damper's or MR damper's highly nonlinear dynamic behavior: parametric modeling and non-parametric modeling. Numerous parametric models can be easily established to simulate an ER or MR damper, by an appropriate combination of springs and viscous dashpots, such as Bingham model, BingMax model, nonlinear viscoelastic model, Bouc-Wen model, etc.

Bingham plastic model and extended Bingham model, as shown in Fig. 2.1 and Fig. 2.2, were widely employed to describe the behavior of MR fluids (Makris et al. 1996). However, it assumed that the fluid remained rigid in the pre-yield region. Thus, the Bingham model did not describe the fluids elastic properties at small deformations and low shear rate that is necessary for dynamic applications.

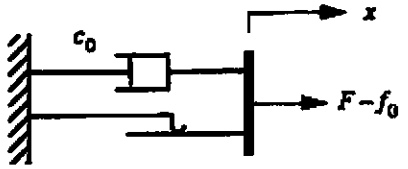

Fig. 2.1 Binham model of controllable damper

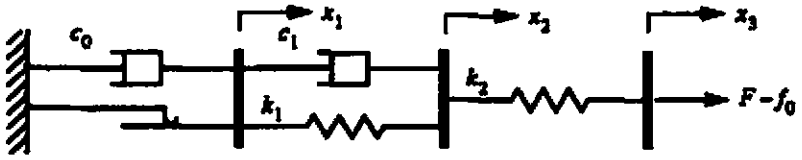

Fig. 2.2 Extended Binham model

Bingmax model was composed of a Maxwell element and a Coulomb friction element as depicted in Fig. 2.3. Kamath and Wereley (1997) combined two linear shear flow mechanisms with nonlinear weighting functions to model the MR damper.

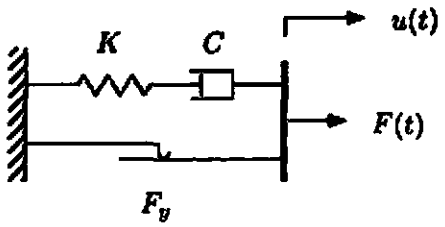

Fig. 2.3 BingMax model

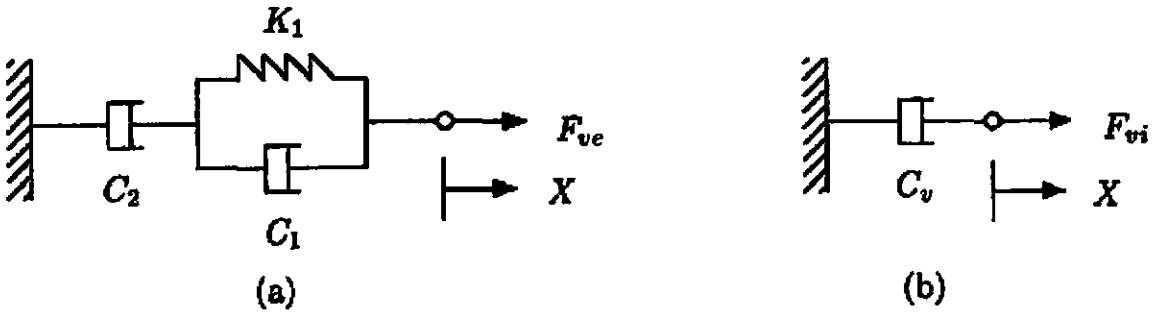

Fig. 2.4 Viscoelastic plastic model (a) Viscoelastic mechanism (b) Viscous mechanism

Ehrgott and Masri (1992) used a Chebyshev polynomial fit to approximate the force generated by an ER test device. Neural network (NN) was used to simulate the dynamic behavior of MR dampers (Chang and Roschke 1998). Fuzzy logic controller (FLC) has been developed and successfully applied in various tests of different structures, including base isolation system, half-scale multistory buildings, etc, (Kim and Rosche 2005).

2.2 Bouc-Wen Model

The Bouc-Wen model, as illustrated in Fig. 2.5, can well predict the force-

displacement and the force-velocity relationship of the damper. However, the simple Bouc-Wen model can not well simulate the highly nonlinear force-velocity behavior, either, in the region where the acceleration and velocity have opposite signs and the velocity is small. Therefore, Spencer et al. (1997) proposed a modified Bouc-Wen model, as shown in Fig. 2.6, and this model outperformed other models after a quantitative study of errors compared with the experimental data. Yang et al. (2002) further considered the dynamic response time of MR damper, and a current driver has been shown to be effective in reducing its response time.

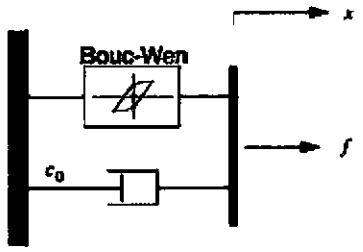

Fig. 2.5 Simple Bouc-Wen model

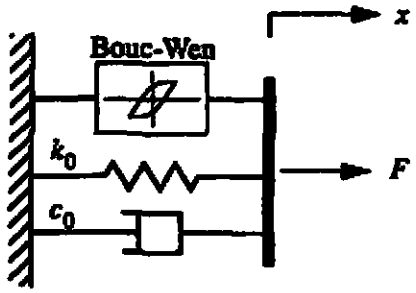

Fig. 2.6 Modified Bouc-Wen model

Song and Kiureghian (2006) proposed a generalized Bouc-Wen model to describe highly asymmetric hysteresis with applicability to nonlinear time-history analysis and nonlinear random vibration analysis by use of the equivalent linearization method (ELM). This new model offered enhanced flexibility in shape control by introducing an equation that describes the relation between the shape-control parameters and the slopes of the hysteresis loop in different phases.

Based on widely used Bouc-Wen model, Wang and Chang (2007) developed a generalized biaxial smooth hysteresis model that took into account the commonly

observed hysteretic characteristics of strength and stiffness degradation, asymmetry in ultimate positive and negative forces, pinching and those exclusively found in biaxial interaction.

Wang and Willatzen (2007) constructed a differential-equation model for hysteresis using a nonlinear second-order differential equation on the basis of a nonconvex potential energy. Both the third- and fifth- order nonlinear terms were investigated and it was shown that the fifth-order nonlinearity was able to give a perfect prediction of experimental hysteretic behaviors. The hysteretic behavior of an MR damper and the polarization hysteresis in piezoelectric materials were modeled and used as testing examples.

2.3 Some Properties of Bouc-Wen Model

For the simple Bouc-wen model shown in the Fig. 2.5, the equations governing the damping force f are as follows

$$f = c_0\dot{x} + \alpha z \tag{2.1}$$

$$\dot{z} = -\gamma|\dot{x}|z|z|^{n-1} - \beta\dot{x}|z|^n + A\dot{x} \tag{2.2}$$

where x =displacement, $\dot{x}$ = velocity, $c_0 = c_{0a} + c_{0b}u$, $\alpha = \alpha_a + \alpha_b u$, u = commanding voltage, z = the evolutionary variable that accounts for the history dependence of the response; γ , β and A are parameters of Bouc-Wen model.

For example, assume $n = 1, A = 1.0$ and $\gamma = \beta = 0.5$, the energy dissipation per cycle of oscillation as a function of force amplitude z_0 is:

$$D(z_0) = 2\int_0^{z_0} \frac{zdz}{1-z} - z_0^2 \tag{2.3}$$

In addition, equation (2.2) can be written as when $n=1$

$$\dot{z}=-\gamma|\dot{x}|z-\beta\dot{x}|z|+A\dot{x} \tag{2.4}$$

Directly expand equation (2.4) into six sub-equations, then directly solve them as follows:

I. $\dot{x}>0, z>0, \frac{dz}{dx}=-(\gamma+\beta)z+A \Rightarrow z=z[x(t)]=\frac{A}{\gamma+\beta}+e^{-(\gamma+\beta)\cdot x(t)}\cdot c_1(t)$

II. $\dot{x}>0, z<0, \frac{dz}{dx}=-(\gamma-\beta)z+A \Rightarrow z=z[x(t)]=\frac{A}{\gamma-\beta}+e^{-(\gamma-\beta)\cdot x(t)}\cdot c_1(t)$

If $\gamma=\beta$, then $z=z[x(t)]=A\cdot x(t)+c_1(t)$

III. $\dot{x}<0, z>0, \frac{dz}{dx}=(\gamma-\beta)z+A \Rightarrow z=z[x(t)]=-\frac{A}{\gamma-\beta}+e^{(\gamma-\beta)\cdot x(t)}\cdot c_1(t)$

If $\gamma=\beta$, then $z=z[x(t)]=A\cdot x(t)+c_1(t)$

IV. $\dot{x}<0, z<0, \frac{dz}{dx}=(\gamma+\beta)z+A \Rightarrow z=z[x(t)]=-\frac{A}{\gamma+\beta}+e^{(\gamma+\beta)\cdot x(t)}\cdot c_1(t)$

V. $\dot{x}=0$, then $\dot{z}=0$, $c_1(0)=z(0)=0$ (Assume $z(0)=0$) $\Rightarrow z[x(t)]=z(0)$

VI. $\dot{x}\neq 0$ and $z=0, \frac{dz}{dx}=A \Rightarrow z=z[x(t)]=A\cdot x(t)+c_1(t)$, and $c_1(0)=z(0)-A\cdot x(0)$

Based on the six different expressions of $z(t)$, it is possible to solve the constant $c_1(t)$ from the values of foregoing moment. The constant $c_1(t)$ must be a time-variant variable, although it is not directly related with x and z. Therefore, it would be promising if we can further derive the time series of constant $c_1(t)$, thus solve $z(t)$.

2.4 Semi-active Control Algorithms

Semi-active control schemes act in a desirable fashion in both a passive and an active mode, with generally enhanced performance. Leitmann (1994) treated two

cases, one in which the properties of the spring and damper can be varied separately, and the other in which these properties can be varied only jointly. Two control schemes were considered, one based on minimizing the rate of change of the energy of the body and the other based on consideration of Lyapunov stability theory. The first control scheme appeared to be superior to the other in decreasing phase amplitude and in suppressing resonance effects.

Yang et al. (1994) generalized the linear quadratic regulator (LQR) control theory for seismic-excited linear structures. Spencer et al. (1994) discussed frequency domain optimal control strategies for active control of building structures under seismic loadings. The two specific techniques, H_2 and H_∞ control methods, were given. Sadek and Mohraz (1998) summarized the previous work about semi-active control algorithms for variable dampers in reducing the seismic response.

Jansen and Dyke (2000) presented the results of a study to evaluate the performance of a number of proposed semi-active control algorithm for use with multiple MR dampers, including control based on Lyapunov controller algorithm, decentralized Bang-Bang control, maximum energy dissipation method, clipped-optimal control and modulated homogeneous friction algorithm. The conclusions showed that Lyapunov controller algorithm, clipped-optimal control and modulated homogeneous friction algorithm achieved significant reductions in the responses. Herein the former two algorithms are discussed in details because they have been widely applied in numerical calculation and model tests. The fuzzy logic controller (FLC) is also introduced, considering that researchers in the several large-scale tests

have adopted it.

2.4.1 Lyapunov Controller Algorithm

This algorithm is classified as a bang-bang controller and depends on the sign of measured force and the state of the system (Leitmann 1994; Jansen and Dyke 2000).

Consider the Lyapunov function:

$$V(x) = \frac{1}{2}\|x\|_P \tag{2.5}$$

where $\|x\|_P = \left[x^T P x\right]^{1/2}$ is P -norm of states, and P is real, symmetric, positive definite matrix, derived from

$$PA + A^T P + Q = 0 \tag{2.6}$$

The derivative of equation (2.5) is

$$\frac{d}{dt}V(x(t)) = \nabla V(x(t))\dot{x}(t) \tag{2.7}$$

Considering

$$L(u) = x^T PAx + x^T PBu + xPE\ddot{x}_g \tag{2.8a}$$

and

$$L(u(t)) = \frac{d}{dt}V(x(t)) \tag{2.8b}$$

, therefore

$$\dot{V} = -\frac{1}{2}x^T Qx + x^T PBf + x^T PE\ddot{x}_g \tag{2.9}$$

Because only the middle term that contains the force f affects the selection of voltages, the control law minimizing $\dot{V}$ is

$$\dot{V} = V_{\max} H((-x^T)PB_i f_i) \tag{2.10}$$

where $H(\cdot)$ is heave step function; f_i is measured force produced by the i^{th} MR

damper; B_i is the i^{th} column of the B matrix. One challenge is in the selection of an appropriate Q matrix.

2.4.2 Clipped-optimal Controller

Clipped-optimal control has been successfully applied in numerical study and model test of structural control using MR dampers (Jansen and Dyke 2000; Yi et al. 2001). Consider a seismically excited structure controlled with n MR damper, and assume that the forces provided by the control devices are adequate to keep the response of the primary structure from exiting the linear region. The vector of measured control forces is $f = [f, f, ..., f_n]^T$, and the vector of desired control forces is $f_c = [f_{c1}, f_{c2}, ..., f_{cn}]^T$ based on the measured structural responses y and the measured control force vector f applied to the structure; that is

$$f_c = L^{-1}\left\{-K_c(s)\begin{Bmatrix} y \\ f \end{Bmatrix}\right\} \tag{2.11}$$

where, $L\{\cdot\}$ = Laplace transform; $K_c(s)$ = control law.

For these applications, the measurements typically available for control force determination include the absolute acceleration of selected points on the structure, displacement of each control device, and measurement of each control force.

Two preconditions are made based on the model of the MR damper discussed previously:

- The control voltage to the i th device is restricted to the range $v_i = [0, V_{\max}]$.
- For a fixed set of states, the magnitude of the applied force $|f_i|$ increases when v_i

increases and decreases when v_i decreases.

Based on these assumptions, the command voltage is set to maximum level ($v_i = V_{max}$) when the measured force f_i is less than the desired force f_{ci}. When $|f_i| > |f_{ci}|$, the command voltage is set to zero. Even when the measured force and the desired force do not have the same sign, the voltage is also set to zero. In other words, MR damper are switched between "On" and "Off". This control law can be graphically shown as in Fig. 2.7, and concisely expressed in a mathematical form:

$$v_i = V_{max} H\left((f_{ci} - f_i) \cdot f_i\right) \tag{2.12}$$

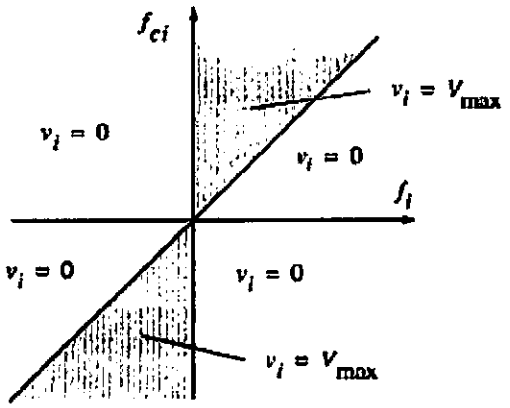

Fig. 2.7 Graphical view of clipped-optimal control

However, clipped optimal control appears not efficient. An inverse dynamic model that can directly relate damper force f_i to input voltage was proposed by Tse and Chang (2004). The applicability and the accuracy of this inverse model were testified in the experiments of prototype MR damper. This model can provide a smoother tracking of the desired force and was considered as an alternative means of commanding the MR damper. However, this inverse model highly depended on the accuracy of Bouc-wen model. Therefore, clipped controller was still a simple yet

effective model if Bouc-Wen model was not available.

Tsang et al. (2006) developed a simplified inverse dynamics (SID) models for MR fluid dampers with respect to both the Bingham plasticity and the Bouc-Wen hysteresis model, mainly based on time-continuity properties. This proposed SID model was a simple, yet powerful tool for emulating the optimal control force, consuming little computational effort.

2.4.3 Fuzzy Logic Controller

The fuzzy logic controller has attracted our attention in recent years because of its inherent robustness and ability to handle nonlinearities and uncertainties (Battaini et al. 1998; Symans and Kelly 1999; Schurter and Roschke 2000; Ahlawat and Ramaswamy 2001)

Chang and Zhou (2002) used neural networks to emulate the inverse dynamics of MR damper, showing that MR damper can be commanded to follow the desired control force closely. Zhou et al. (2003) proposed an adaptive fuzzy control strategy that involves the design of a fuzzy controller and an adaptation law.

A fuzzy logic controller (FLC) was used to modulate the MR damper and a genetic algorithm (GA) was used to optimize the FLC for smart base isolation with a novel friction pendulum system (FPS) bearings. The proposed method can find optimal fuzzy rules and the GA-optimized FLC outperforms not only a passive control strategy but also a human-designed FLC and a conventional semi-active control algorithm (Kim and Roschke 2006). Full-scale experiments of a combination

of the FPS bearings and the MR dampers were carried out and this combination offered significant possibilities for reduction of displacement and acceleration under a wide variety of seismic loads. Simulation using neuron-fuzzy models of MR damper and FPS bearing predicted the response of hybrid base isolation system very well (Kim et al. 2006; Lin et al. 2006).

CHAPTER 3 Control Method and Tracking Strategies

3.1 State-Space Model

The equations of motion of the building are given by

$$M\ddot{x} + C\dot{x} + Kx = -M\Gamma\ddot{x}_g + \Lambda f \tag{3.1}$$

where $\ddot{x}_g$ = 1D ground acceleration or excitation; f = vector of control forces; Γ = vector of ones; Λ = matrix defining how the control forces are exerted on the structure.

The above equations can be written in the state space form as

$$\dot{z} = Az + Bf + E\dot{x}_g \tag{3.2-a}$$

$$y = Cz + Df \tag{3.2-b}$$

where $z = [x^T, \dot{x}^T]^T$, state vector (here z is different from the one defined in Bouc-Wen model); $y = [\ddot{x}_a^T, x^T]^T$, vector of measured outputs; and

$$A = \begin{bmatrix} 0 & I \\ -M^{-1}K & -M^{-1}C \end{bmatrix};\ B = \begin{bmatrix} 0 \\ M^{-1}\Lambda \end{bmatrix};\ E = -\begin{bmatrix} 0 \\ \Gamma \end{bmatrix};$$

$$C = \begin{bmatrix} -M^{-1}K & -M^{-1}C \\ I & 0 \end{bmatrix};\ D = \begin{bmatrix} M^{-1}\Lambda \\ 0 \end{bmatrix}$$

3.2 Optimal Control Method

3.2.1 Continuous Linear Quadratic Regulator (LQR)

In this section, consider the linear time-invariant system (Lewis 1986)

$$\dot{x} = Ax + Bu \tag{3.3}$$

where $x \in R^n, u \in R^m$ with the associated quadratic performance index

$$J(t_0)=\frac{1}{2}x^T(T)\cdot S(T)\cdot x(T)+\frac{1}{2}\int_{t_0}^{T}[x^T(t)\cdot Q\cdot x(t)+u^T(t)\cdot R\cdot u(t)]dt \tag{3.4}$$

With the time interval set on $[t_0,T]$, we shall determine the control $u^*(t)$ on $[t_0,T]$ that minimizes J for two cases: fixed final state and free final state. In the former case, $u^*(t)$ will turn out to be open-loop control, and the latter case is a closed-loop feedback control. Q is a $2n \times 2n$ positive semi-definite response weighting matrix and R is a $q \times q$ positive definite control force weighting matrix.

The Hamiltonian is

$$H(t)=\frac{1}{2}\left(x^TQx+u^TRu\right)+\lambda^T\left(Ax+Bu\right) \tag{3.5}$$

where $\lambda(t)\in R^n$ is an undetermined multiplier.

The state and the costate equations are

$$\dot{x}=\frac{\partial H}{\partial \lambda}=Ax+Bu \tag{3.6}$$

$$-\dot{\lambda}=\frac{\partial H}{\partial x}=Qx+A^T\lambda \tag{3.7}$$

The control input is

$$0=\frac{\partial H}{\partial u}=Ru+B^T\lambda \;\Rightarrow u(t)=-R^{-1}B^T\lambda(t) \tag{3.8}$$

The given initial state is $x(t_0)$, and the final state $x(T)$ is free. Thus, the terminal condition is

$$\lambda(T)=S(T)\cdot x(T) \tag{3.9}$$

To find such an intermediate state $S(T)$, differentiate the costates to get

$$\dot{\lambda}=\dot{S}x+S\dot{x}=\dot{S}x+S(Ax-BR^{-1}B^TSx) \tag{3.10}$$

Now, taking into consideration the costate equation, we have

$$-\dot{S}=A^TS+SA-SBR^{-1}B^TS+Q \tag{3.11}$$

This is a matrix Riccati equation. Furthermore, define the Kalman gain as

$$K(t) = R^{-1}B^T S(t) \tag{3.12}$$

So the control input can be written as

$$u(t) = -K(t) \cdot x(t) \tag{3.13}$$

In terms of the Kalman gain, the Riccati equation can be written as

$$-\dot{S} = A^T S + SA - K^T RK + Q \tag{3.14}$$

It should be noted that semi-active LQR algorithm has been extensively used for active control (Chu et al. 2005).

3.2.2 Software Implementation of the LQ Regulator

Although the solver *ode45* in MATLAB can be employed in simulations now, some special notes about the software implementation are still presented here.

In the discrete case, the Riccati equation is a simple backward recursion that can be easily programmed. However, in the continuous case, the Riccati equation must be integrated backward. Most Runge – Kutta integration routines run forward in time. Therefore, the best way is to first convert equation (3.14) into one that is forward integrable. The complete simulation procedure is shown in Fig. 3.1 (Lewis 1986).

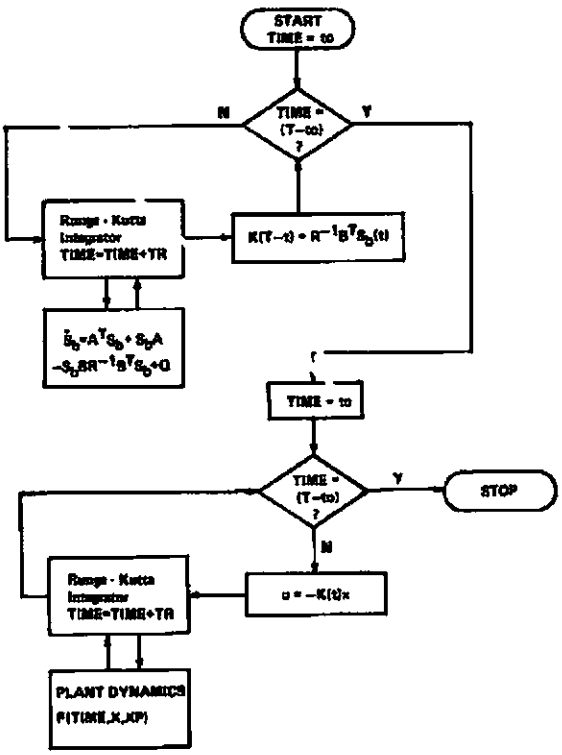

Fig. 3.1 Continuous LQ regulator simulation procedure

3.3 Two Different Tracking Strategies

The differential equations governing the constrained vibration of SDOF system as well as the corresponding control force due to an MR damper are

$$\ddot{x}+2\xi\dot{x}+\omega^2 x=-\frac{f}{m}-\ddot{x}_g \tag{3.15}$$

$$f=c_0\dot{x}+\alpha z \tag{3.16}$$

where x is displacement, ξ is damping ratio, ω is frequency, f is control force, c_0 and α are parameters of Bouc-Wen model.

Then, the above ordinary differential equations can be expressed in state-space model, in two different forms:

(1) Modified inverse dynamic model

$$\frac{dy_1}{dt} = y_2$$
$$\frac{dy_2}{dt} = -(2\xi\omega + c_0)\cdot y_2 - \omega^2 y_1 - \alpha y_3 - \ddot{x}_g \tag{3.17}$$
$$\frac{dy_3}{dt} = -\gamma|y_2|y_3 - \beta y_2|y_3| + Ay_2$$

If y_1 and y_2 are both $n\times1$ scalars and y_3 represents $m\times1$ force, the preceding equations can also be used to simulate a MDOF system.

(2) Direct method

$$\frac{dy_1}{dt} = y_2$$
$$\frac{dy_2}{dt} = -(2\xi\omega + c_0)\cdot y_2 - \omega^2 y_1 - \alpha y_3 - \ddot{x}_g \tag{3.18}$$

where $y_1 = x$, $y_2 = \dot{x}$, $y_3 = z$, and therefore, y_3 can be obtained directly from these equations.

An example is given to compare the effectiveness and accuracy of both methods. In this example, the properties of an assumed stiff one-story building are: mass m = 0.227 N/cm/s2, stiffness k = 297 N/cm, damping coefficient ξ = 0.01. The corresponding parameters of Bouc-Wen model are introduced in Section 2.3, and in this example, they are: α_a = 27.3 N/cm, α_b = 26.5 N/cm·V, c_{0a} = 0.032 N·s/cm, c_{0b} = 0.02 N·s/cm·V, A = 120, γ = 300 cm^{-1} and β = 300 cm^{-1}.

In addition, the time interval is 0.01 second in the following numerical calculation, and the time lag is not considered herein.

3.3.1 Based on a Modified Inverse Dynamic Model

Compared with clipped optimal controller, the advantages of commanding an

intermediate voltage in this new strategy include: (1) result in a potentially more effective vibration control; (2) avoid the overuse of MR damper, thus elongate their life; (3) save electricity energy for MR damper.

Semi-active control of building structures is essentially an optimal control problem that forces the structures to track a desired force f_{ci} over a specified time interval. As stated in the preceding sections, the LQR is selected as the optimal control law. However, in real application, the MR damper cannot always achieve such a desired/optimal control force. Normally the damper is limited by its capacity, the maximum damping force that it can provide.

As illustrated in Fig. 1.1, a modified inverse dynamic model has been developed to adjust the voltage u_{i+1} at $t(i+1)$ in order to track the optimal/desired damper force f_{ci} at $t(i)$, when compared with the damping force f_i at $t(i)$. The predicted damper force f_{i+1} at $t(i+1)$ can be obtained using the Bouc-Wen model after the voltage u_{i+1} has been determined.

In order to obtain the desired force, the evolutionary variable z_i at time $t(i)$ in the Bouc-Wen model is evaluated. Then the determined voltage $\hat{u}_{i+1}$ at time $t(i+1)$ can be expressed as follows:

$$\hat{u}_{i+1} = \frac{f_{ci} - c_{0a} \cdot \dot{x}_i - \alpha_a \cdot z_i}{c_{0b} \cdot \dot{x}_i + \alpha_b \cdot z_i} \tag{3.19}$$

In this way, we can appropriately direct the damper to an intermediate voltage, not just a maximum or minimum value, in order to generate a specific damping force. The main advantage of this strategy is its simplicity and practicability. In the mathematical model, the physical properties of MR damper, especially pre-yielding

and post-yielding behavior, are fully considered and effectively simulated. This physical property can be represented by the evolutionary variable z_i, and it should be always limited by the ultimate hysteretic strength z_u (Chang and Zhou 2002), which is expressed as

$$z_u = \mathrm{sgn}(\dot{x})\left(\frac{A}{\gamma+\beta}\right)^{1/n}, |z_i| \le |z_u| \tag{3.20}$$

Thus, this assumption is also utilized in the following numerical calculations.

In fact, the optimal/desired force f_{ci} at $t(i)$ in simulation represents the actual damping force f_{act}, as can be directly obtained from the test. Together with the actual voltage u_i from the test, the evolutionary variable z_{i+1} can be calculated by solving equation (3.19), if this is a real-time monitoring and no time delay has occurred. In practice, this new control strategy provides a fast and reliable way to identify $\hat{u}_{i+1}$, and we no longer need to solve differential equations.

For example, from the stiff one-story building of Section 4.2, we can get the time series of displacement, absolute acceleration and voltages, as well as the plot of displacement x-z.

3.3.2 Direct Method

From the equations, the relationship between $z(t)$ and $x(t)$ in the Bouc-Wen model is simple and solvable when $n=1$. Therefore, we can directly calculate the coefficient $c_1(t)$, thus $z(t)$ can be directly obtained after the constant $c_1(t)$ has been determined.

In order to achieve the semi-active control of one-story buildings using an MR damper, the corresponding codes have been written to compare their efficiency. In the both cases, $z(t)$ will be solved by *ode45* solver or directly from the equations, and this is the basic difference between two methods.

From Fig. 3.2 and Fig. 3.3, we can see:

- Generally, the time history of displacements is very close as expected, although there is some discrepancy between them.
- The reason why there exists such discrepancy may be numerical error between two methods.
- Moreover, the evolutionary variable $z(t)$ always ranges from –0.2 to +0.2.

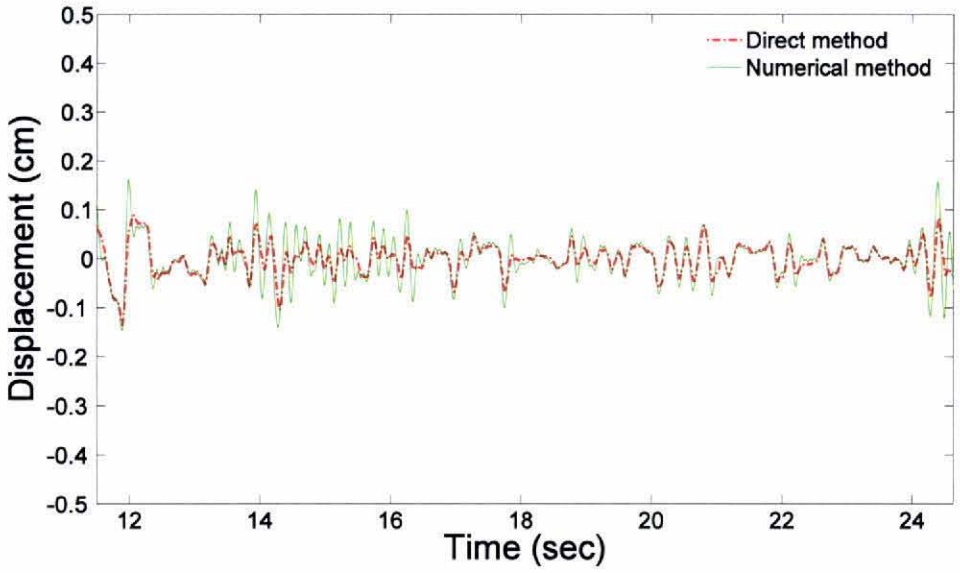

Fig. 3.2 Comparison of displacements of stiff one-story building using one MR damper

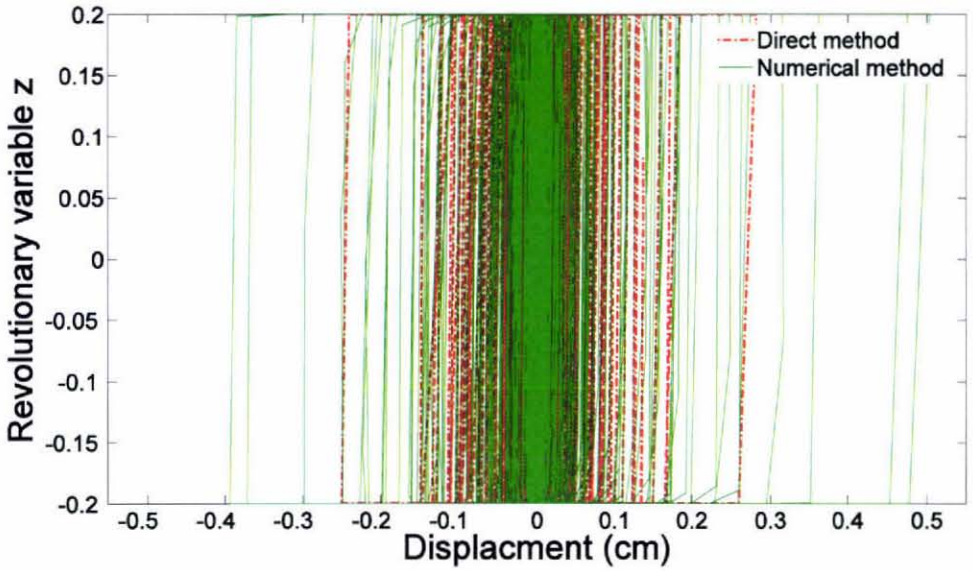

Fig. 3.3 Comparison of $x-z$ relationship

However, it should be noted that the direct method is applicable only when $n=1$. When $n=2$, it is impossible to find the exact solution to equation (2.2). Therefore, the numerical method based on this modified inverse dynamic model is an effective way when $n \geq 2$. Moreover, it appears that more economic and efficient way is to utilize *ode45* solver of MATLAB.

In addition, from the plot of $z(x)$, the slope of this set of curves always equals 120 ($=\frac{A}{\gamma+\beta}$). Therefore, this relationship can be further used to simplify the six sub-cases in Section 2.3, and possibly implementing a tracking strategy by assuming $z(x)=\frac{A}{\gamma+\beta}x+C1$.

CHAPTER 4 Case Study

4.1 Uncontrolled Case and Controlled Cases

Uncontrolled case refers to the case where no control device is applied, thus no control force. Controlled cases include passive-on case, passive-off case, ideal case and the controlled case in which MR damper is commanded using this new strategy. Passive-on case represents maximum voltage applied to the MR damper, "On" state. Passive-off case indicates that the voltage is set to minimum, "Off" state. Ideal case assumes that optimal damping forces derived from LQR method can be achieved and will be directly employed in the numerical calculation.

White Gaussian noise (WGN) and 1940 El Centro earthquake are chosen as excitations. WGN is a random signal with a flat power spectral density, and it is a good approximation of many real-world situations and generates mathematically tractable models. 1940 El-Centro earthquake is widely adopted by civil engineering industry as benchmark excitation.

Herein, the structural control of SDOF system (one-story building) is firstly studied under WGN and El-Centro earthquake. Moreover, the control efficiencies of MR damper on stiff, moderate and flexible one-story buildings are compared and discussed.

Finally, this strategy is also applied to a six-story building.

4.2 Case Study: One-story Building

The properties of three assumed buildings are shown in Table 4.1.

Table 4.1 Properties of different one-story buildings

	Stiff	Moderate	Flexible
Mass	m_i	m_i	m_i
Stiffness	k_i	$k_i/16$	$k_i/100$
Frequency	ω_i	$\omega_i/4$	$\omega_i/10$
Period	T_i	$4T_i$	$10T_i$

where mass, m_i= 0.227 N/cm/s^2; stiffness, k_i= 297 N/cm; frequency, $\omega_i = \sqrt{k_i/m_i}$; period, $T_i = \frac{2\pi}{\omega_i}$.

WGN and 1940 El-Centro earthquake are scaled to different amplitudes in the following numerical calculations to represent slight, moderate and strong earthquake. In section 4.2.1, the responses of stiff one-story building excited by the El-Centro earthquake are obtained, at uncontrolled and controlled case, respectively. This new control strategy proves to effectively reduce the structural responses of buildings.

In section 4.2.2, the stiff one-story building is excited by a randomly generated WGN, and the plots of control ratios versus different R (assume: $Q = 1.0$) are given, using this new control strategy. In addition, calculate the structural responses at ideal case and passive cases. The corresponding results will be compared with those from this new control strategy.

In section 4.2.3, the structural control of a moderate one-story building and a flexible, excited by WGN, is further studied. The performances of MR damper for the three one-story buildings are compared and discussed.

In section 4.2.4 and section 4.2.5, this new strategy is applied to the structural control of stiff, moderate and flexible buildings under El-Centro earthquake.

4.2.1 Validation of the New Control Strategy

Define the control efficiency of structural responses as

$$Ratio = \frac{\text{Uncontrolled response - Controlled response}}{\text{Uncontrolled response}} \tag{4.1}$$

The following responses are considered: peak value of relative displacement, root mean square (RMS) of relative displacement, peak value of absolute acceleration and RMS of absolute acceleration.

The percentage of voltages between minimum and maximum is also defined as

$$Ratio = \frac{\text{Number of intermediate voltages between minimum and maximum}}{\text{Total number of voltages}} \tag{4.2}$$

However, its physical meaning is quite different from the preceding one. In addition, the controlled case in this section corresponds to $(Q, R) = (1, 0.01)$.

From Fig. 4.1 and Fig. 4.2, a 56.8% reduction in peak displacement and a 44.6% reduction in absolute acceleration are observed when compared with the uncontrolled case.

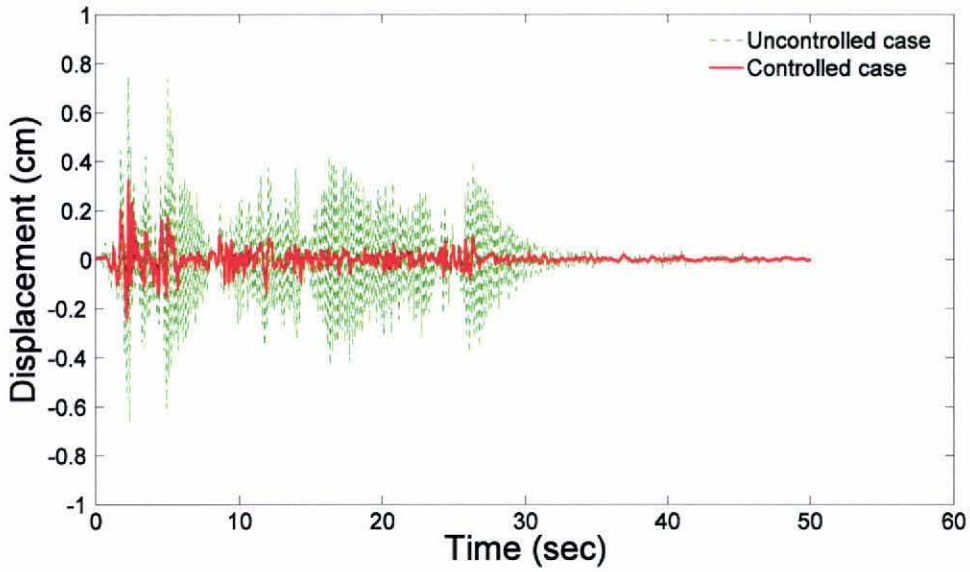

Fig. 4.1 Displacement of stiff one-story building at uncontrolled and controlled cases, excited by El-Centro earthquake

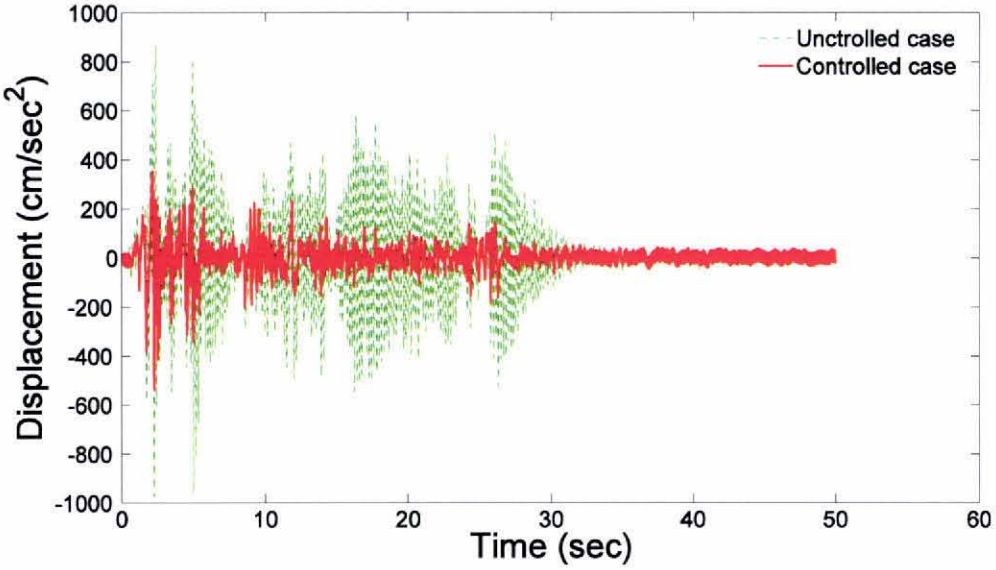

Fig. 4.2 Absolute acceleration of stiff one-story building at uncontrolled and controlled cases, excited by El-Centro earthquake

As shown in Fig. 4.3, the evolutionary variable z ranged from -0.2 to +0.2, as mentioned in Section 3.3.2. The slope of $z(x)$, easily obtained from the plot, is

approximately 120 at several intervals, and this matches well the theoretical value $\frac{A}{\gamma+\beta}$. However, at times, the slop is even greater than the expected value due to the relationship $z = z[x(t)] = \frac{A}{\gamma+\beta} + e^{-(\gamma+\beta)\cdot x(t)} \cdot c_1(t)$, in which the term $e^{-(\gamma+\beta)\cdot x(t)}$ shows exponential growth.

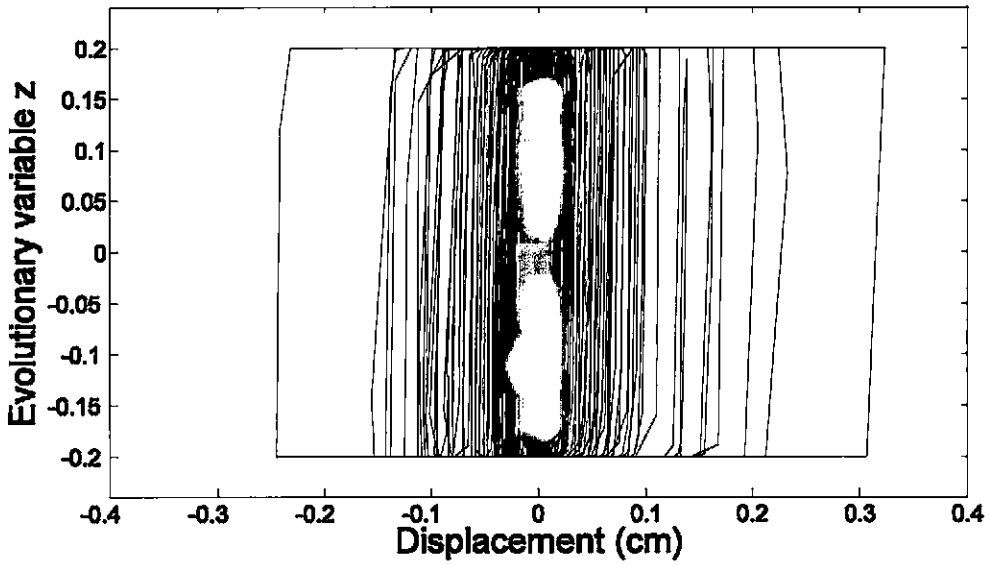

Fig. 4.3 Evolutionary variable z versus displacement x

Fig. 4.4 is the time history of commanding voltage. More than 50% of the total voltages are between minimum voltage (0 V) and maximum voltage (4 V). This shows that it is possible to predict the commanding voltages.

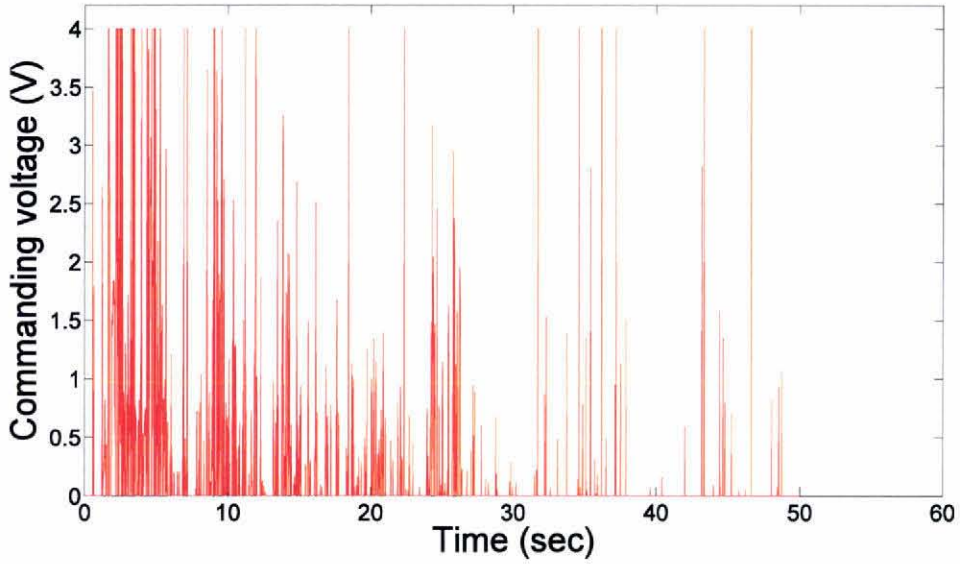

Fig. 4.4 Time history of the commanding voltage

Fig. 4.5 indicates that the MR damper can achieve the desired damping force when the excitation is moderate or low. However, the actual control forces must be limited by the MR damper's capability, and are not related to the amplitudes of excitation.

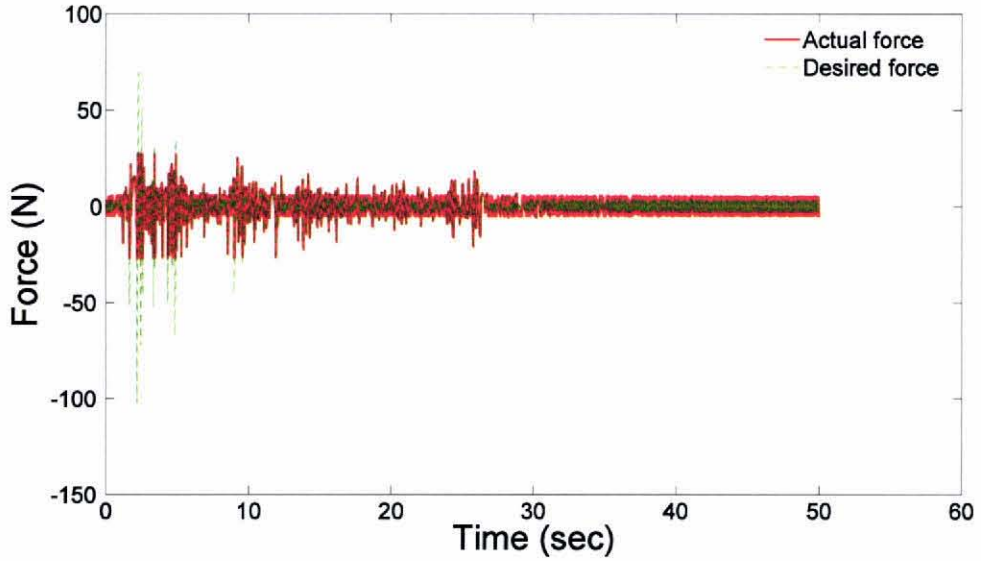

Fig. 4.5 Comparison of the desired damping force and the actual damping force

4.2.2 Stiff One-story Building Excited by WGN

It is observed in Figs. 4.6 - 4.10:

- For displacement, MR damper can achieve around 50% reduction in peak displacement and 20% reduction in RMS displacement.
- The control efficiency almost remains constant except for some fluctuation when R is about 10^{-3}.
- In Fig. 4.8 and Fig. 4.9, the control force can result in the increase of acceleration, as is consistent with the conclusions in other papers (Janson and Dyke. 2000; Yi et al. 2001).
- In Fig. 4.6, the wider solid curve represents ideal case – "LQR method". The control efficiency decreases with the elevation of R, corresponding to the decreasing desired damping force is larger. However, it is observed that there exist some points above this curve, however, some others below. In other words, the MR damper can achieve a better control even than the ideal case, if an appropriate R can be determined. For example, such a R is from $10^{-2.4}$ to 10^{0} when the excitation is two-time WGN, and from $10^{-1.5}$ to 10^{0} when the excitation is five-time WGN.
- As shown in Fig. 4.10, more than 50% of voltages are intermediate values when R is around 10^{-3} - 10^{-1}. Moreover, R within this range always corresponds to considerable reduction in displacement and acceleration.

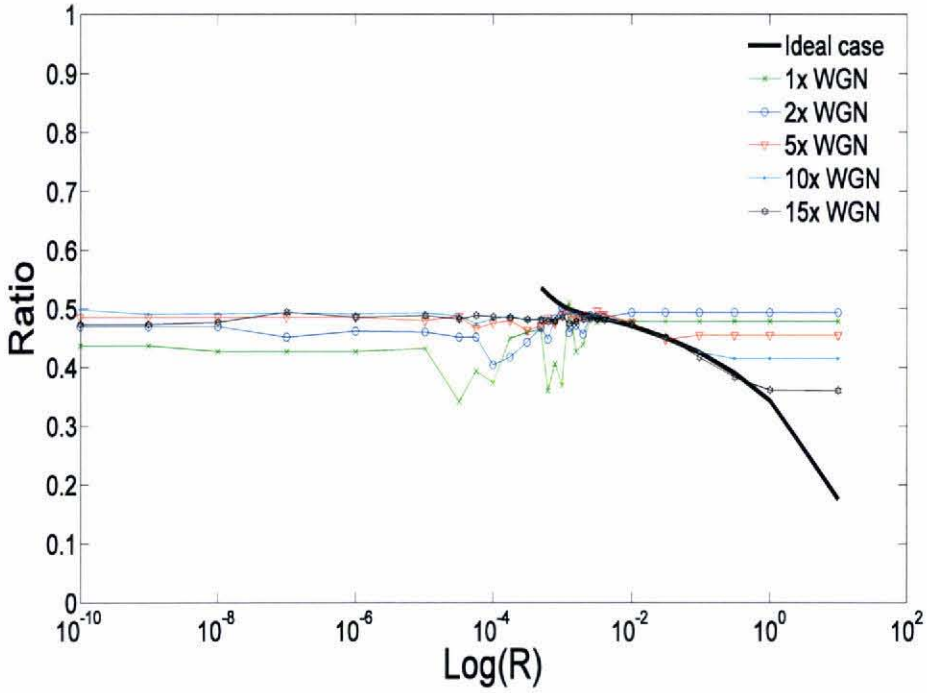

Fig. 4.6 Peak displacement of stiff one-story building excited by different amplitudes of WGN, compared with results derived from LQR method

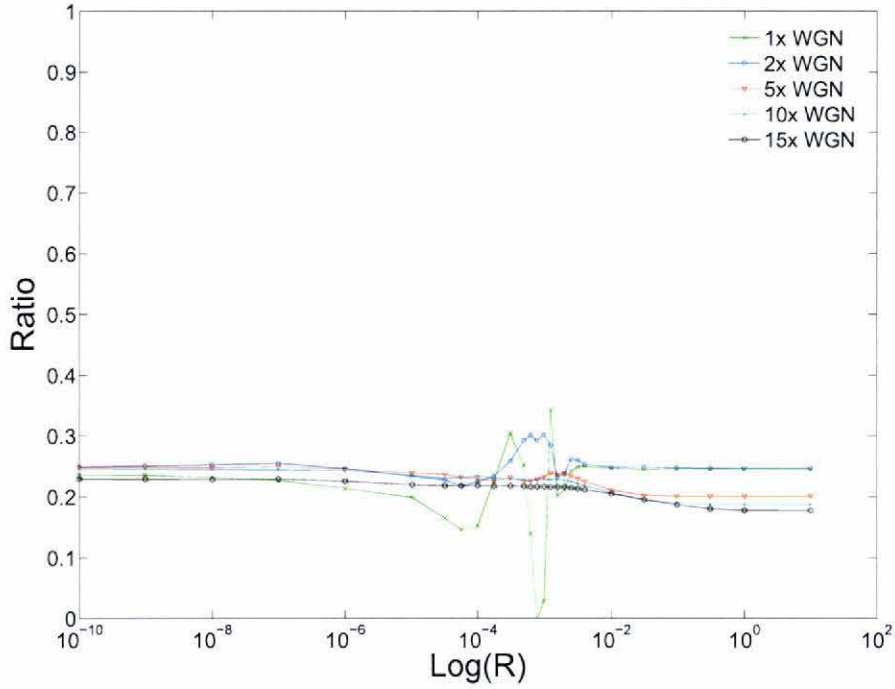

Fig. 4.7 RMS displacement of stiff one-story building excited by different amplitudes of WGN

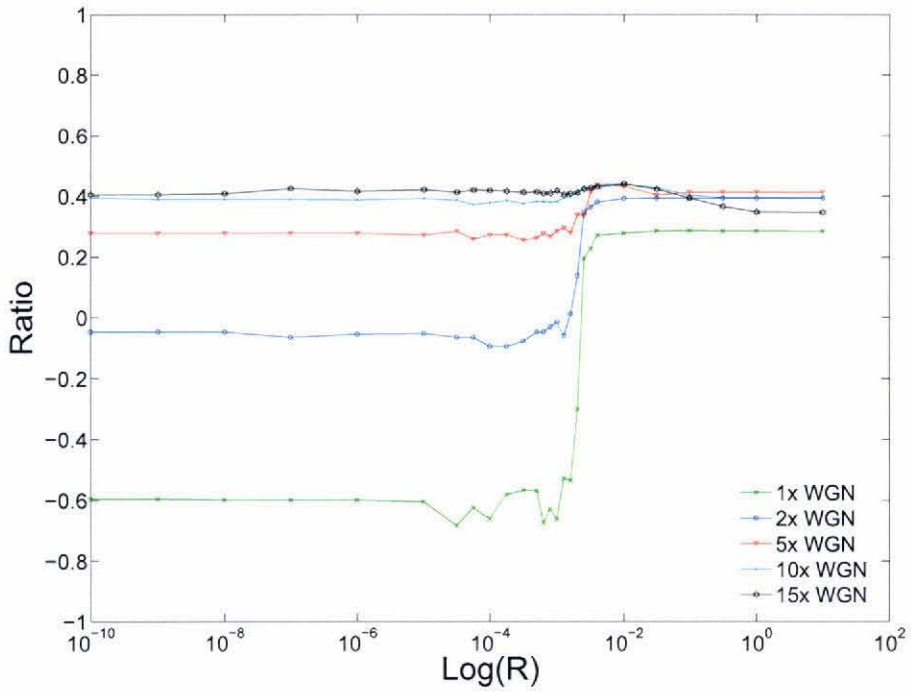

Fig. 4.8 Peak acceleration of stiff one-story building excited by different amplitudes of WGN

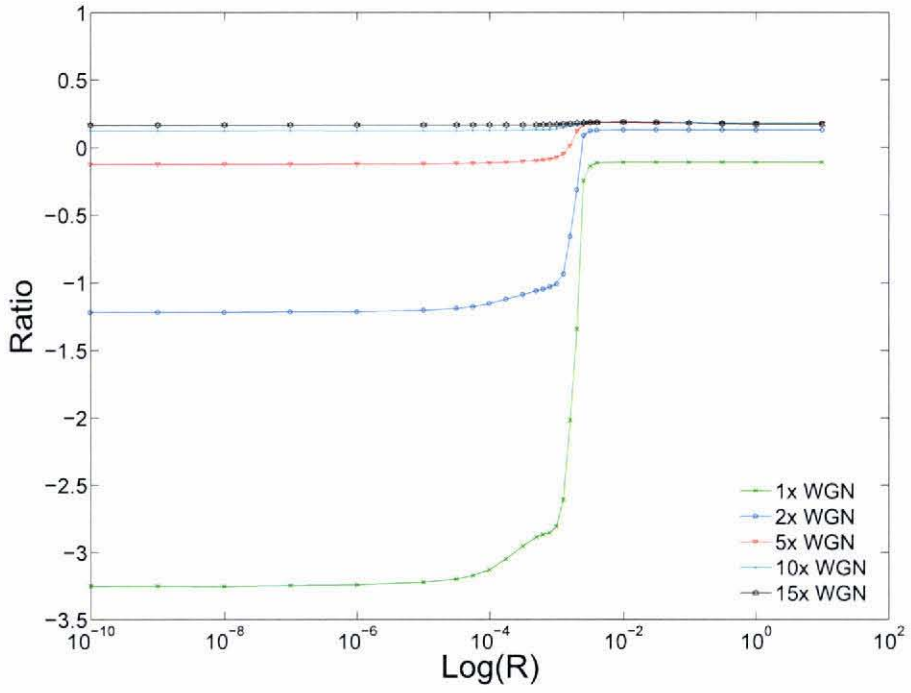

Fig. 4.9 RMS acceleration of stiff one-story building excited by different amplitudes of WGN

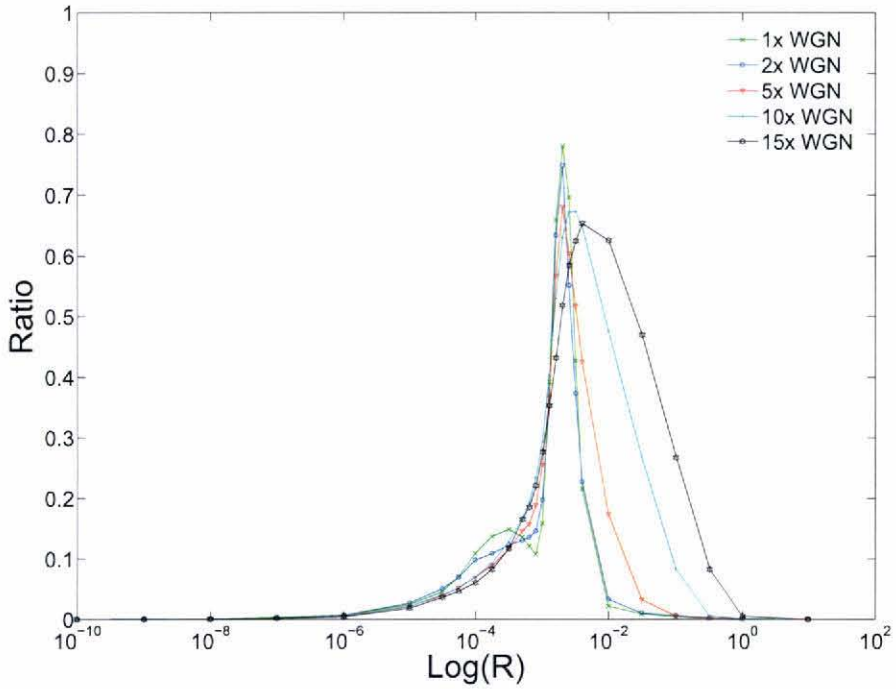

Fig. 4.10 Percentage of voltages between minimum and maximum for stiff one-story building excited by different amplitudes of WGN

As given in Table 4.2, the control efficiencies can be derived at passive-on and passive-off case under each excitation. Graphically, each value in this table represents a straight line in Fig. 4.6.

- Generally speaking, a better control can be observed at passive-on condition than at passive-off condition when the excitation is moderate or strong, except for small amplitude excitation.
- Compared with the curves in Fig. 4.6, the performance of the MR damper is generally bounded by passive-off and passive-on case.
- MR damper performs better in stronger excitation than in slight or moderation excitation, based on the reduction of acceleration. Especially under slight excitation, the control force magnifies the absolute acceleration of the building, as is consistent with results presented by Janson and Dyke (2000).

- Roughly, passive-on control can reduce more displacement and acceleration than passive-off control. However, in some cases, passive-on control produces an excessive damping force, and then results in the increase of acceleration.

Table 4.2 Reduction ratios of responses at passive-cases (excited by WGN)

Response \ Excitation		Slight		Moderate		Strong
		1 × WGN	2 × WGN	5 × WGN	10 × WGN	15 × WGN
Peak Displacement	Passive on	40.30%	44.23%	51.91%	48.42%	48.22%
	Passive off	47.84%	52.30%	45.48%	41.47%	36.05%
RMS Displacement	Passive on	17.35%	21.65%	26.81%	24.53%	21.70%
	Passive off	24.53%	24.63%	20.01%	18.66%	17.82%
Peak Acceleration	Passive on	-62.77%	-7.29%	31.26%	38.06%	41.30%
	Passive off	28.50%	39.38%	41.40%	39.56%	34.64%
RMS Acceleration	Passive on	-372.36%	-140.22%	-12.19%	13.04%	16.78%
	Passive off	-11.10%	12.80%	18.12%	18.11%	17.38%

4.2.3 Moderate and Flexible One-story Buildings Excited by WGN

In this section, the moderate and flexible one-story buildings excited by WGN will be considered respectively. A set of plots of various responses can be obtained finally, including peak displacement, RMS displacement, peak acceleration and RMS acceleration.

Figs. 4.11 - 4.15 are the plots for the moderate building, and Figs. 4.16 - 4.20 correspond to the flexible building. These plots are, to some degree, different from Figs 4.6 - 4.10, the plots of stiff one-story building. From these plots, we find:

- More reduction in displacement can be achieved for moderate and flexible one-

story building, when comparing RMS displacement in Fig 4.7, Fig 4.12 and Fig 4.17. A similar relationship is also applicable for RMS acceleration.

- The trend that the control efficiencies decrease with the increase of R appears more obvious for moderate and flexible one-story buildings than for stiff one-story building.
- More than 50% of voltages are between minimum and maximum values when R is around 10^{-3} - 10^{-1}. A more dispersed distribution can be found for moderate and flexible one-story buildings than that for stiff building. However, for the flexible one-story building, it is difficult to explain why the percentage of intermediate voltages increases with the increase of R, especially when R exceeds 10^{0}.

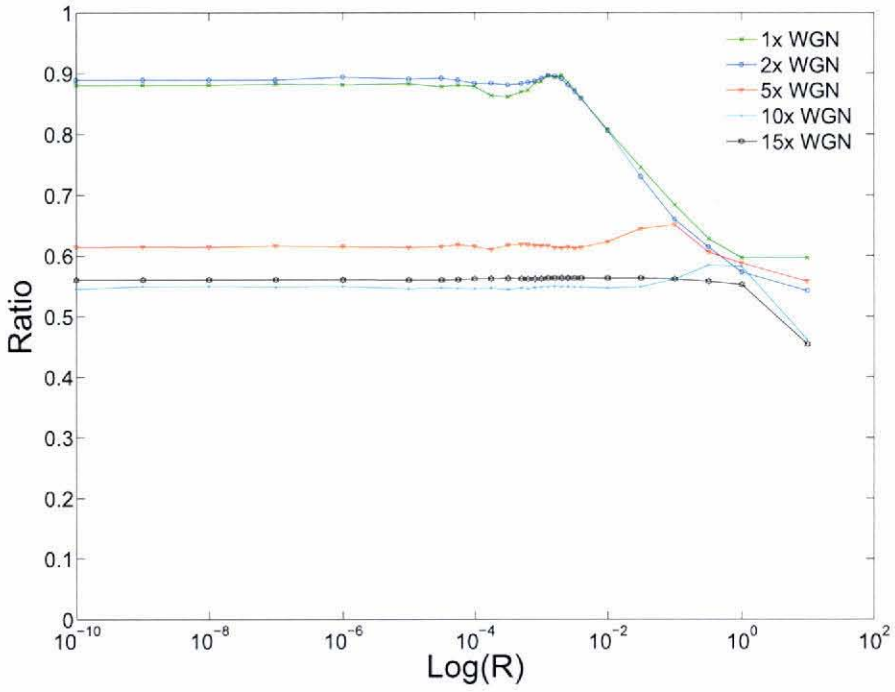

Fig. 4.11 Peak displacement of moderate one-story building excited by different amplitudes of WGN

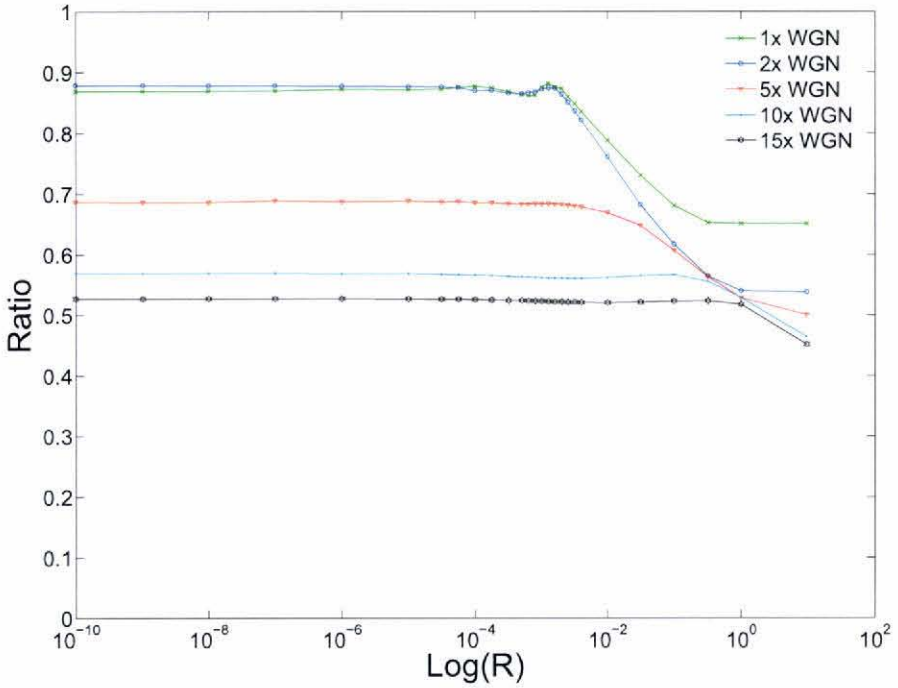

Fig. 4.12 RMS displacement of moderate one-story building excited by different amplitudes of WGN

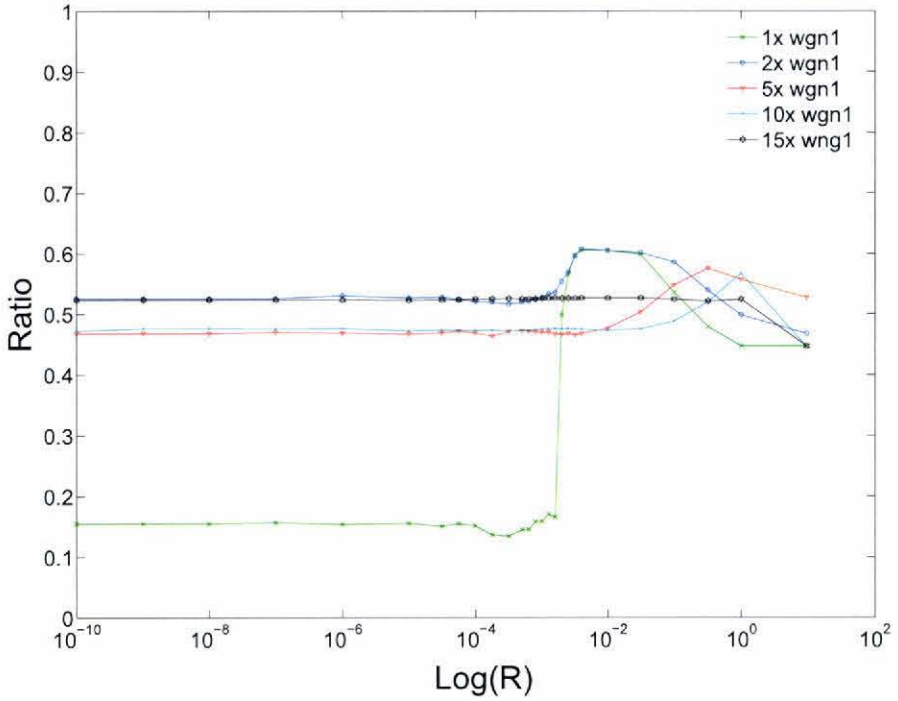

Fig. 4.13 Peak acceleration of moderate one-story building excited by different amplitudes of WGN

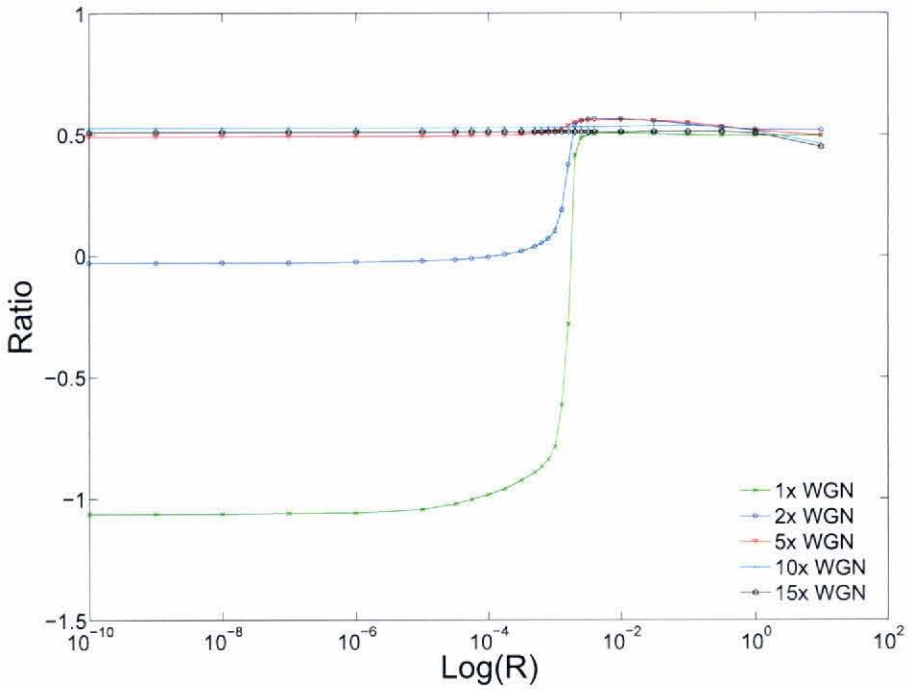

Fig. 4.14 RMS acceleration of moderate one-story building excited by different amplitudes of WGN

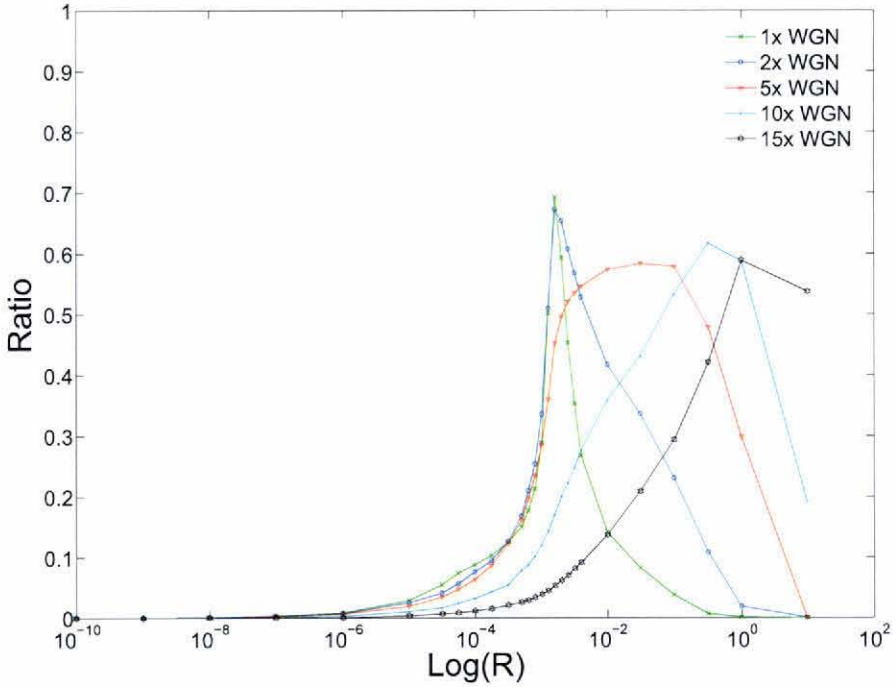

Fig. 4.15 Percentage of voltages between minimum and maximum for moderate one-story building excited by different amplitudes of WGN

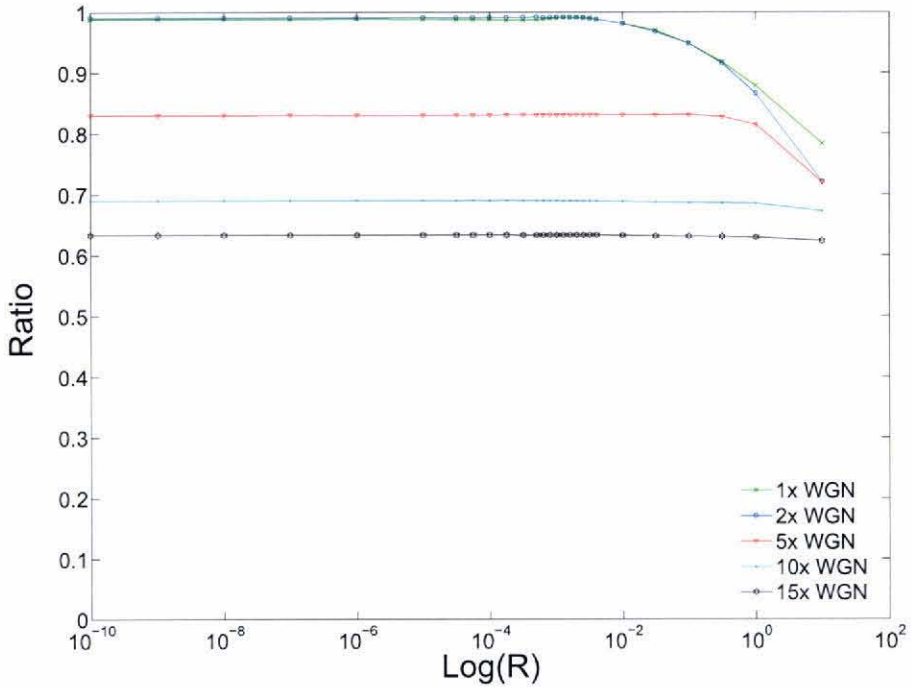

Fig. 4.16 Peak displacement of flexible one-story building excited by different amplitudes of WGN

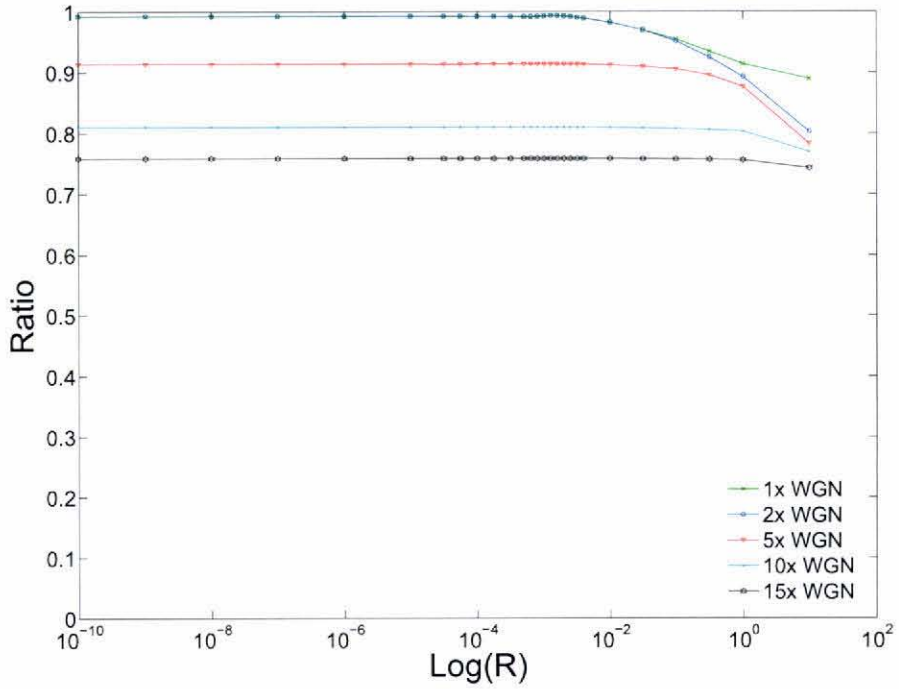

Fig. 4.17 RMS displacement of flexible one-story building excited by different amplitudes of WGN

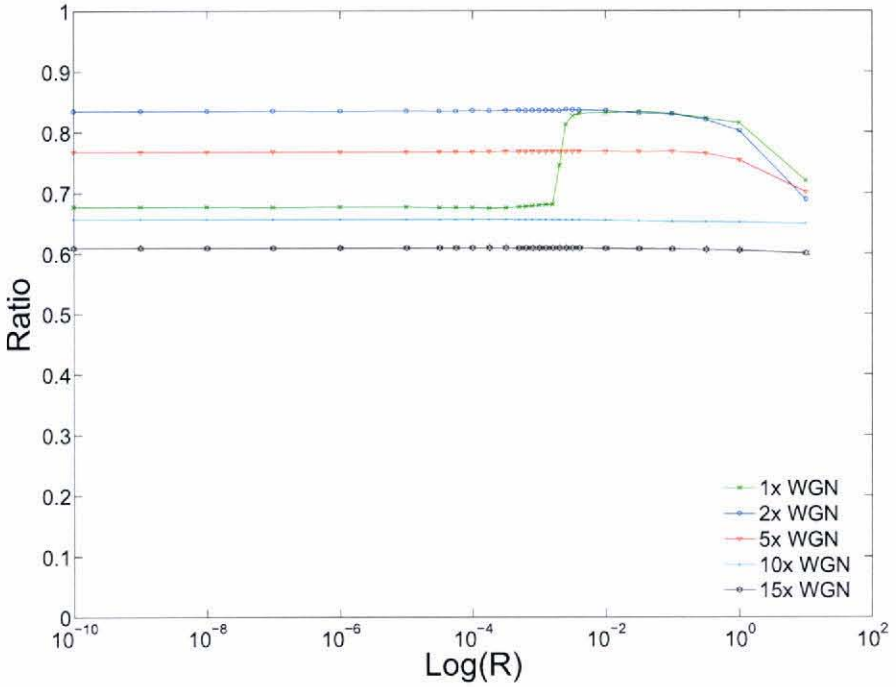

Fig. 4.18 Peak acceleration of flexible one-story building excited by different amplitudes of WGN

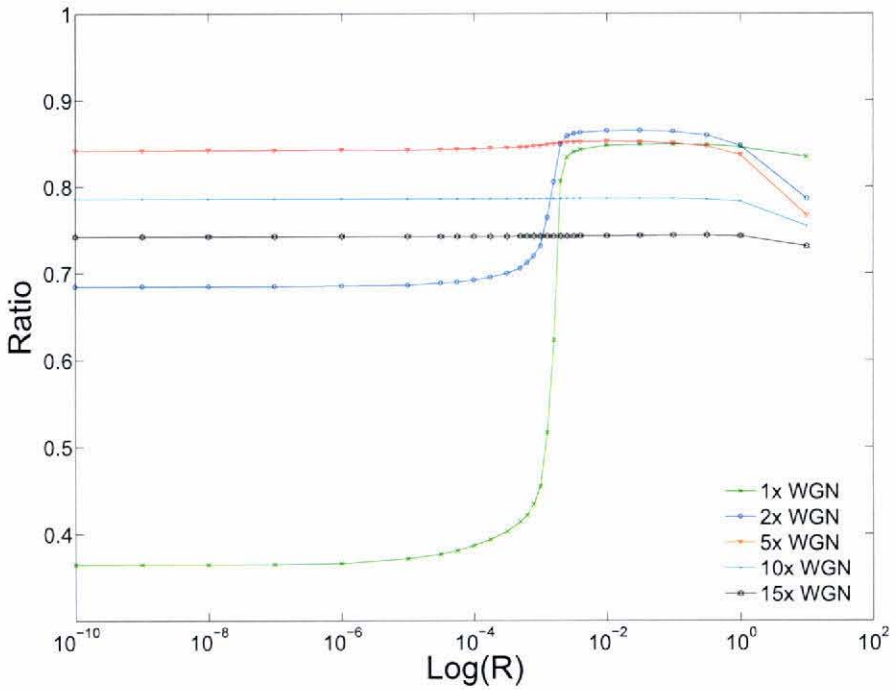

Fig. 4.19 RMS acceleration of flexible one-story building excited by different amplitudes of WGN

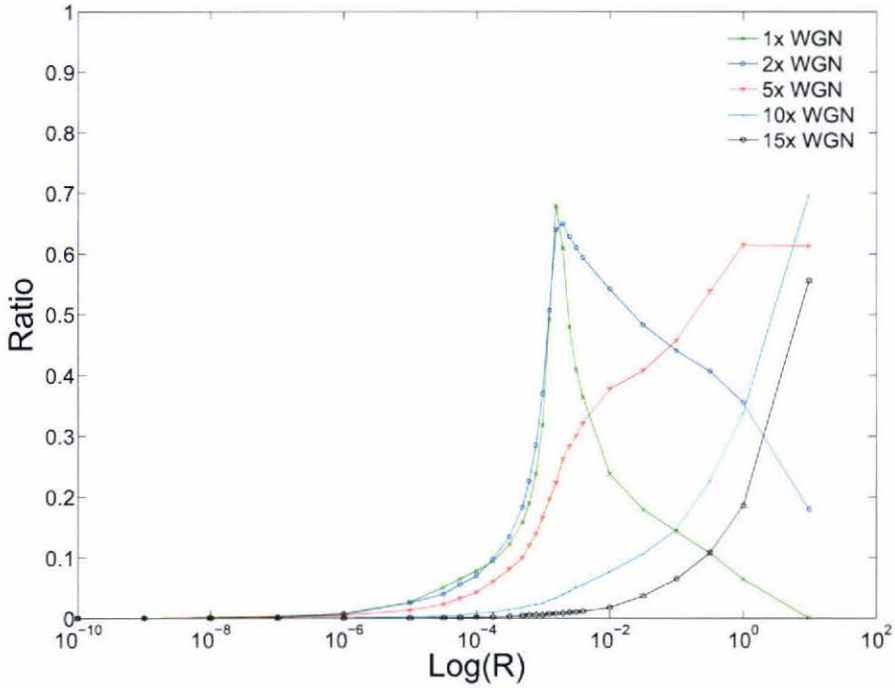

Fig. 4.20 Percentage of voltages between minimum and maximum for flexible one-story building excited by different amplitudes of WGN

4.2.4 Stiff One-story Building Excited by 1940 El-Centro Earthquake

Replacing the WGN with the 1940 EL-Centro earthquake, we can also calculate the responses of the stiff, moderate and flexible one-story buildings. Figs.4.21- 4.25 are the plots of control efficiency of the stiff one-story building.

- For peak displacement, the reductions for each scaled El-Centro earthquake change between 50% and 80%. The differences of ratios for scaled El-Centro earthquakes appear greater than those for scaled WGNs. Moreover, the ratio decreases obviously with increasing R that ranges from 10^{-3} to 10^{0}, however, it keeps almost constant when R is less than 10^{-3}, as shown in both Fig. 4.21 and Fig. 4.22.
- Comparing Fig. 4.23 and Fig. 4.24, the greater amplitudes of earthquake, the

relatively lower control efficiencies of the peak acceleration, on the contrary, the higher control efficiencies found for the RMS acceleration. The reason might be that the peak acceleration is normally governed by extreme values of earthquake; however, the RMS acceleration depends on the whole history of earthquake.

- In contrast, as shown in Fig. 8 and Fig. 9, the plots of peak acceleration and RMS acceleration keep consistent, when the excitation is WGN, with uniform amplitudes and flat power spectral density.
- MR damper can perform a "best" control of all considered responses when R is around $10^{-2.5}$ - $10^{-1.5}$, corresponding the maximum percentage of intermediate voltages, as indicated in Fig. 4.25.

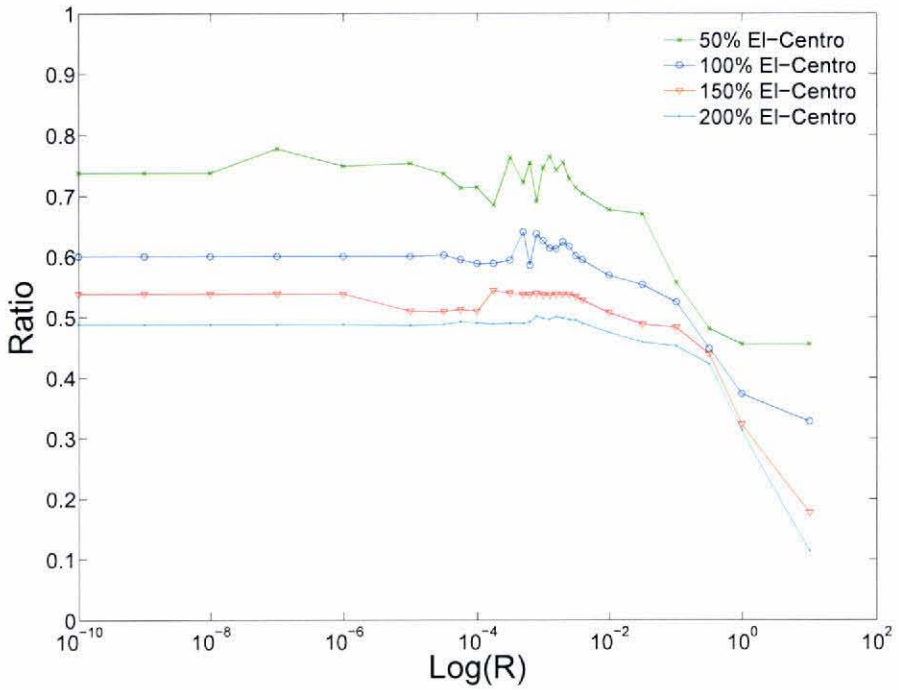

Fig. 4.21 Peak displacement of stiff one-story building excited by different amplitudes of El-Centro earthquake

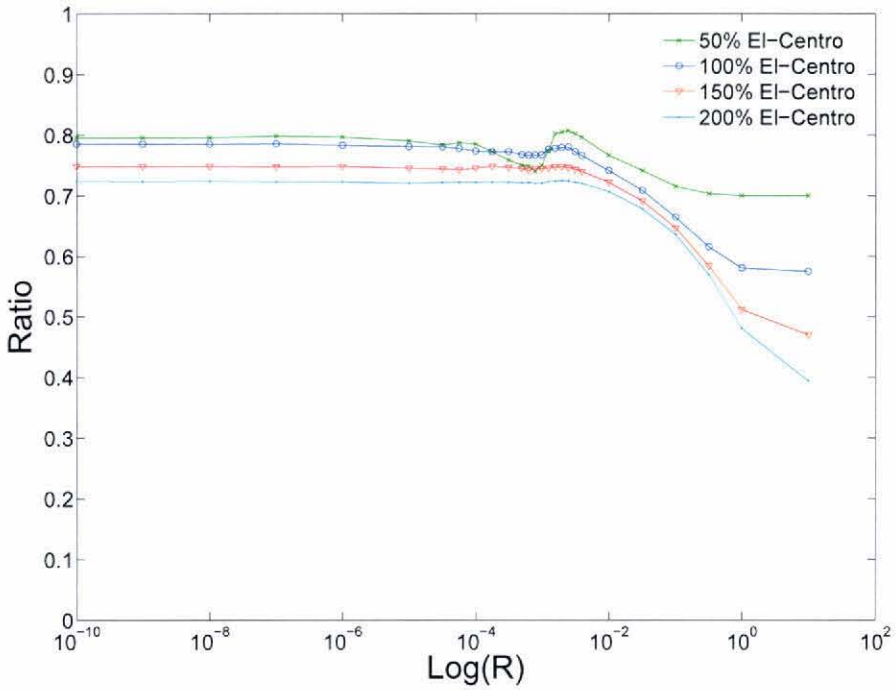

Fig. 4.22 RMS displacement of stiff one-story building excited by different amplitudes of El-Centro earthquake

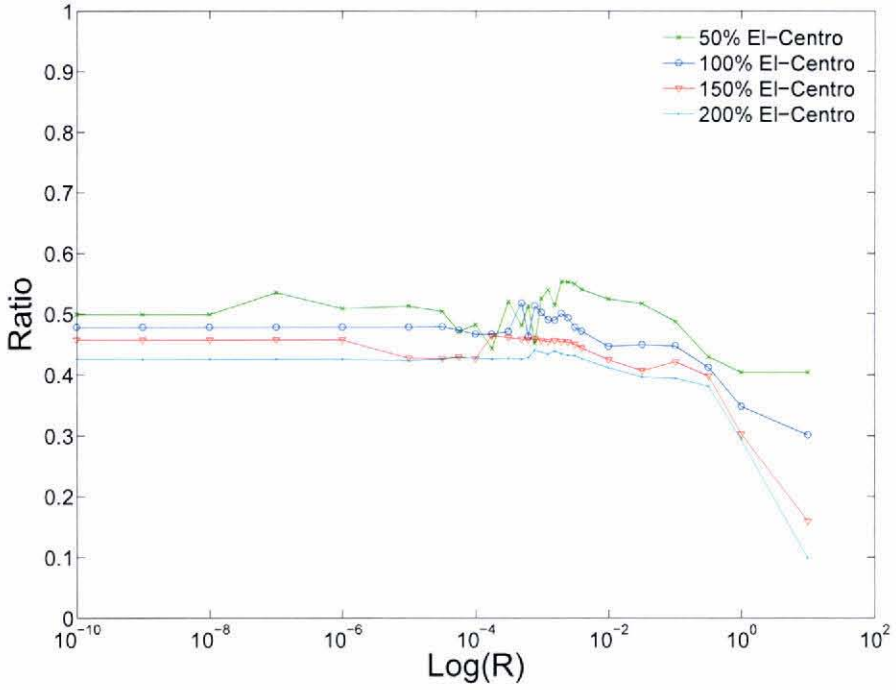

Fig. 4.23 Peak acceleration of stiff one-story building excited by different amplitudes of El-Centro earthquake

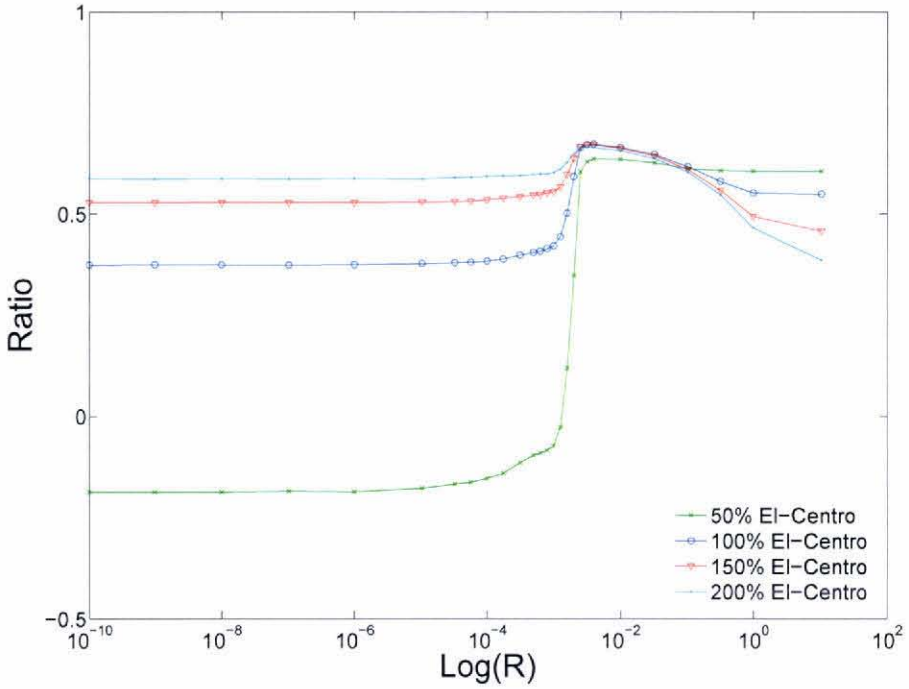

Fig. 4.24 RMS acceleration of stiff one-story building excited by different amplitudes of El-Centro earthquake

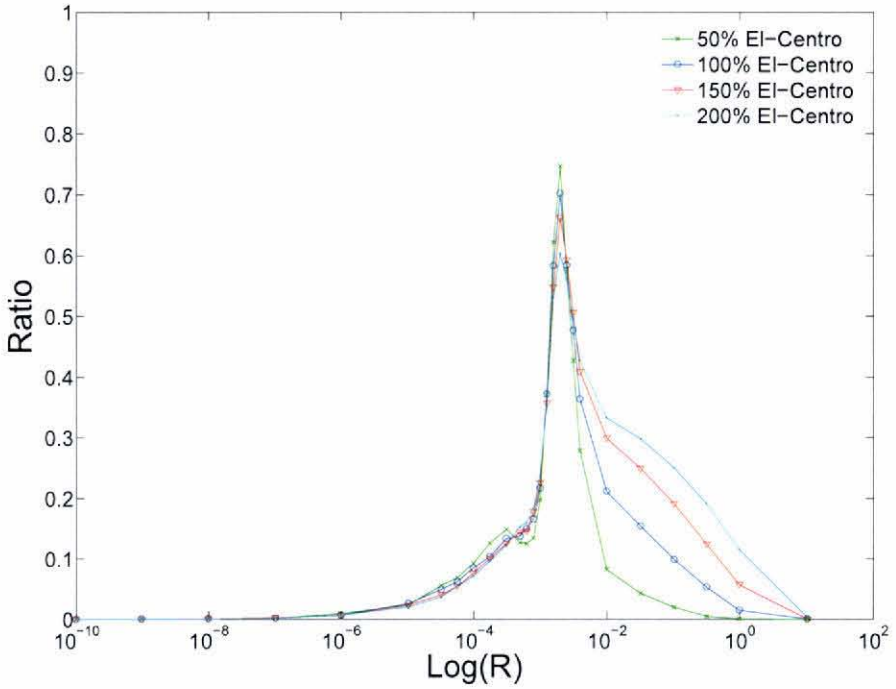

Fig. 4.25 Percentage of voltages between minimum and maximum for stiff one-story building excited by different amplitudes of El-Centro earthquake

4.2.5 Moderate and Flexible One-story Buildings Excited by 1940 El-Centro Earthquake

Fig. 4.26 - Fig. 4.30 are the plots for the moderate one-story building. Fig. 4.31 - Fig. 4.35 are the plots for the flexible one-story building. Through these plots, we can find:

- A higher control efficiency can be achieved for moderate and flexible building using MR damper, comparing the plots of RMS displacement in Fig. 4.21, Fig. 4.26 and Fig. 4.31. The similar trend can be further observed for RMS acceleration.
- Moderate and flexible buildings are more sensible to control force. Therefore, the control force can result in an increase of acceleration for the buildings with smaller stiffness, comparing Fig. 4.24, Fig. 4.29 and Fig 4.34.
- The plots of percentages of intermediate voltages for moderate and flexible one-story buildings are very similar to those of stiff one-story building.

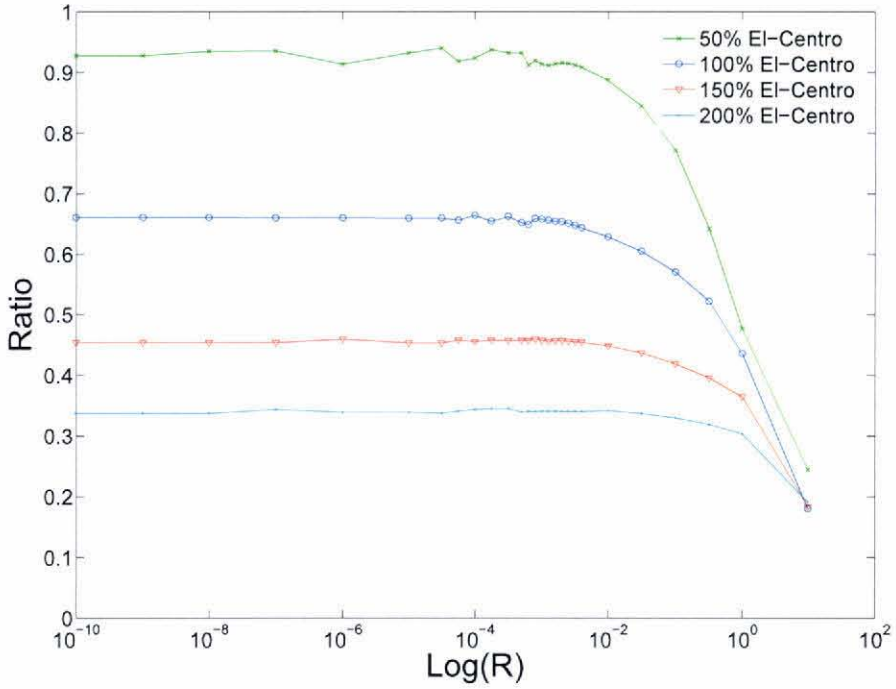

Fig. 4.26 Peak displacement of moderate one-story building excited by different amplitudes of El-Centro earthquake

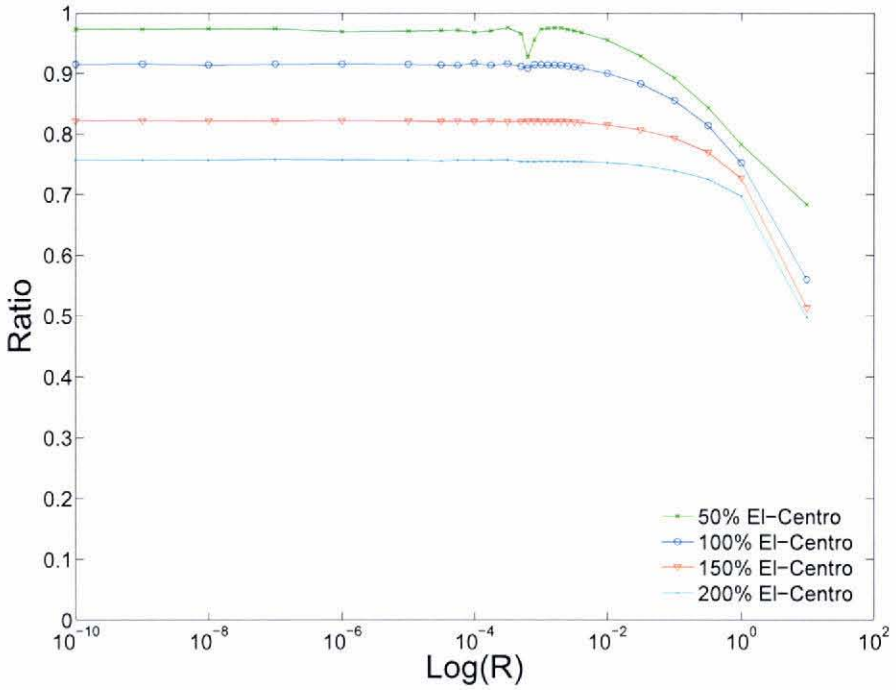

Fig. 4.27 RMS displacement of moderate one-story building excited by different amplitudes of El-Centro earthquake

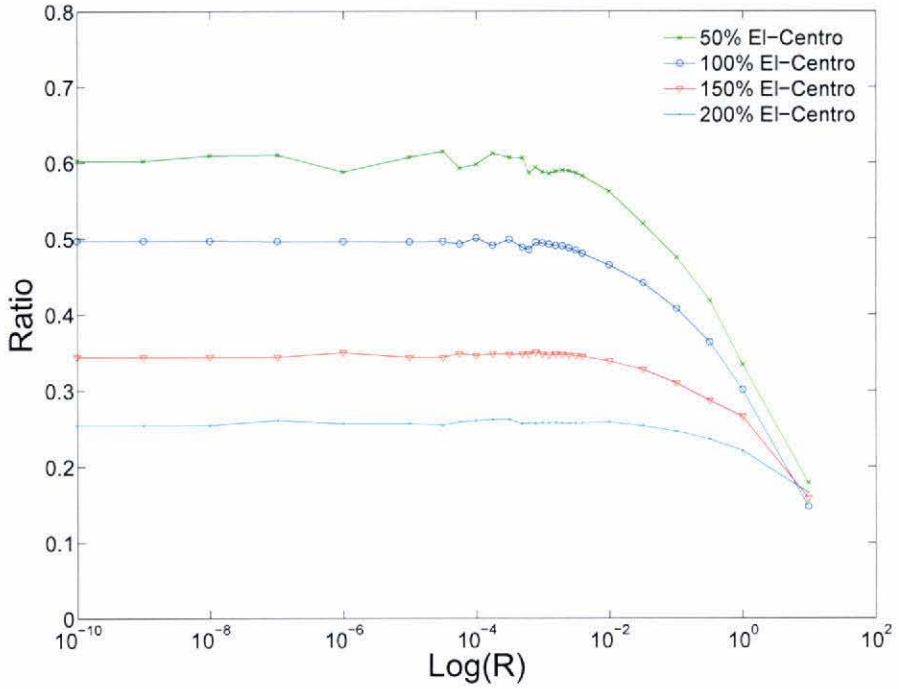

Fig. 4.28 Peak acceleration of moderate one-story building excited by different amplitudes of El-Centro earthquake

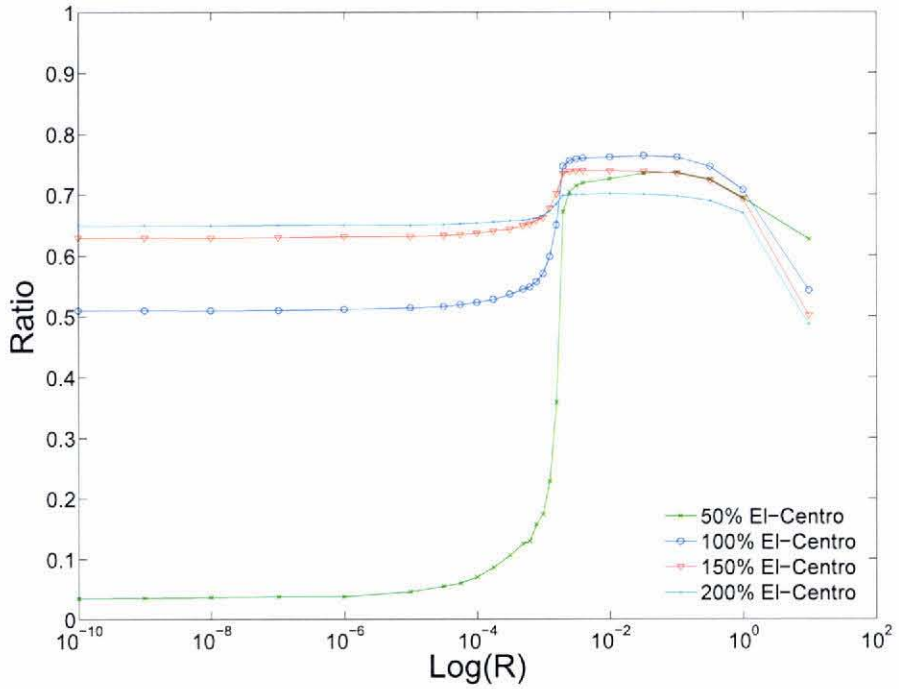

Fig. 4.29 RMS acceleration of moderate one-story building excited by different amplitudes of El-Centro earthquake

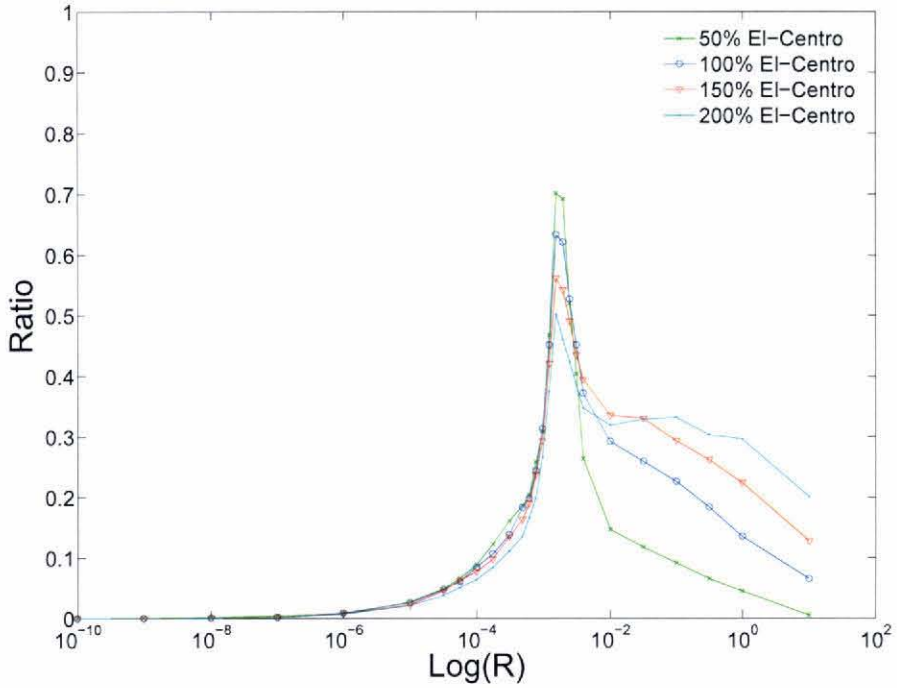

Fig. 4.30 Percentage of voltages between minimum and maximum for moderate one-story building excited by different amplitudes of El-Centro earthquake

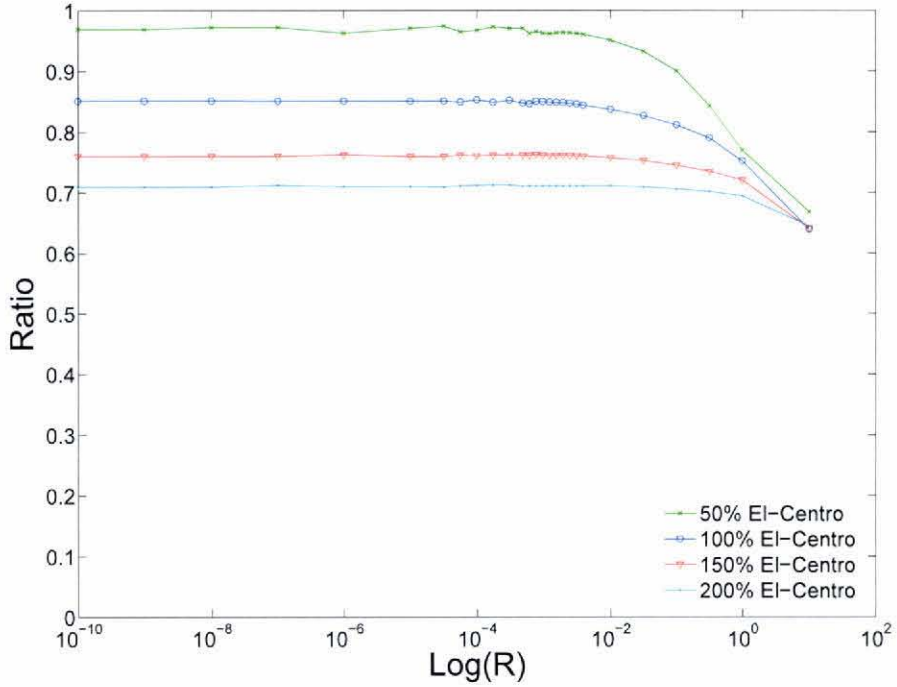

Fig. 4.31 Peak displacement of flexible one-story building excited by different amplitudes of El-Centro earthquake

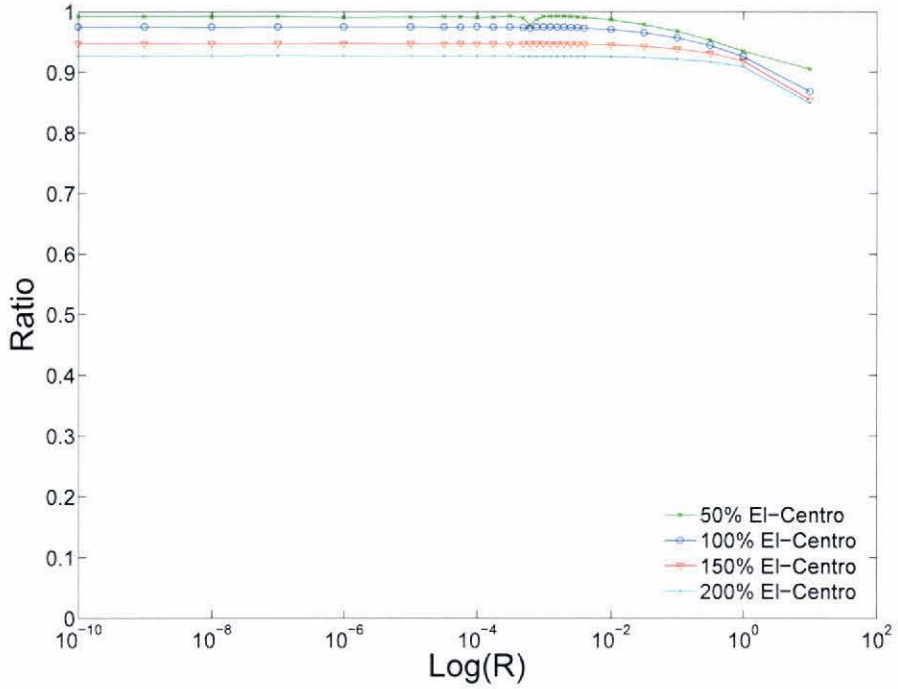

Fig. 4.32 RMS displacement of flexible one-story building excited by different amplitudes of El-Centro earthquake

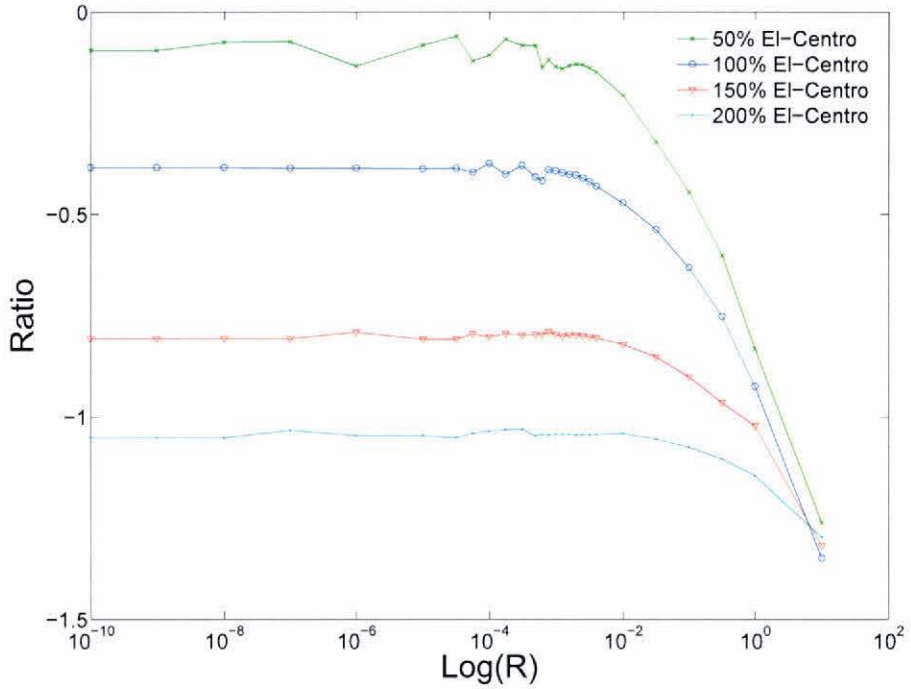

Fig. 4.33 Peak acceleration of flexible one-story building excited by different amplitudes of El-Centro earthquake

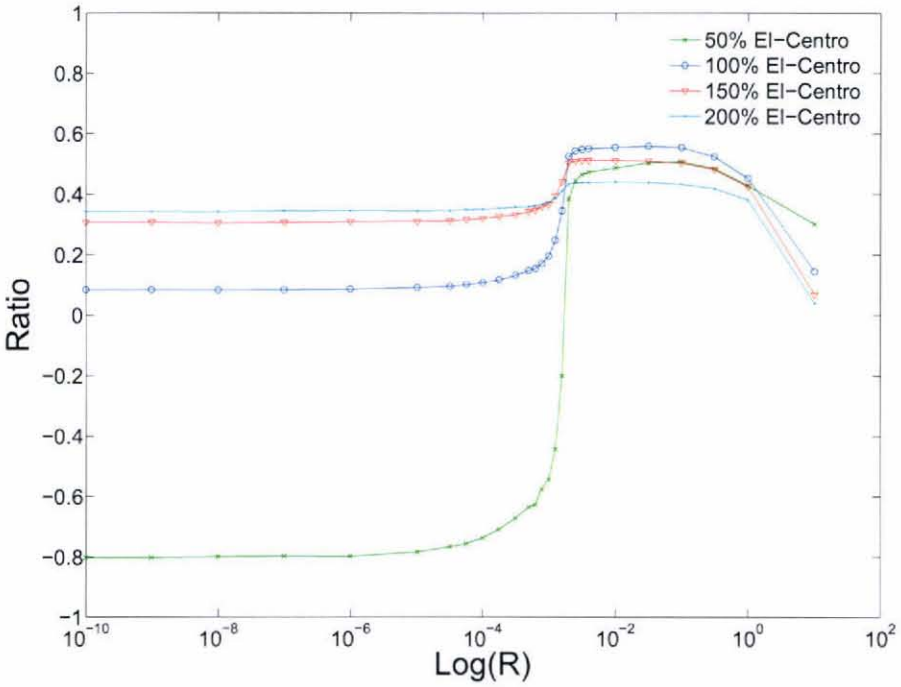

Fig. 4.34 RMS acceleration of flexible one-story building excited by different amplitudes of El-Centro earthquake

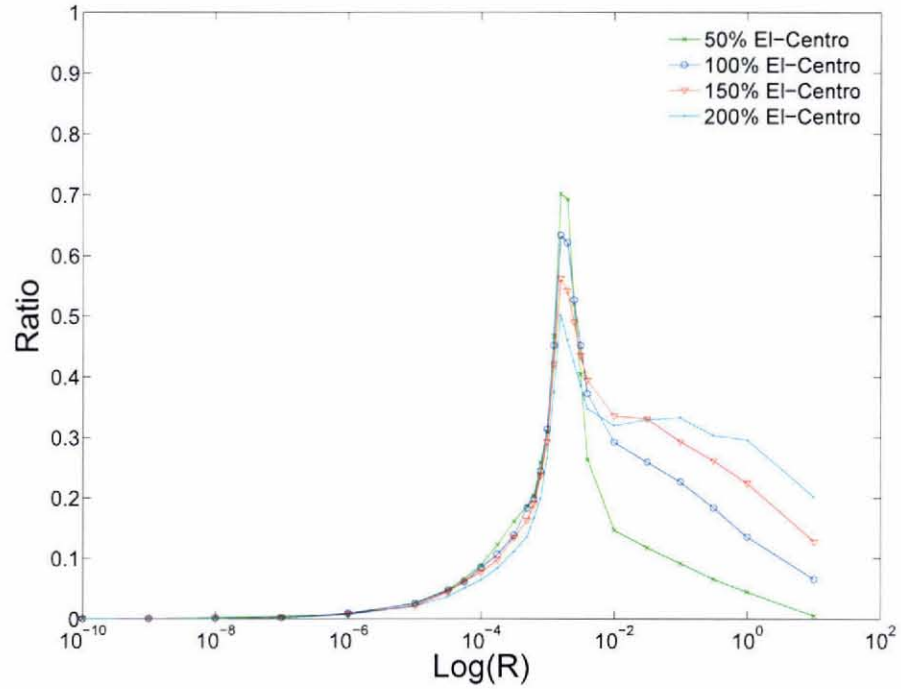

Fig. 4.35 Percentage of voltages between minimum and maximum for flexible one-story building excited by different amplitudes of El-Centro earthquake

4.3 Case Study: Six-story Building

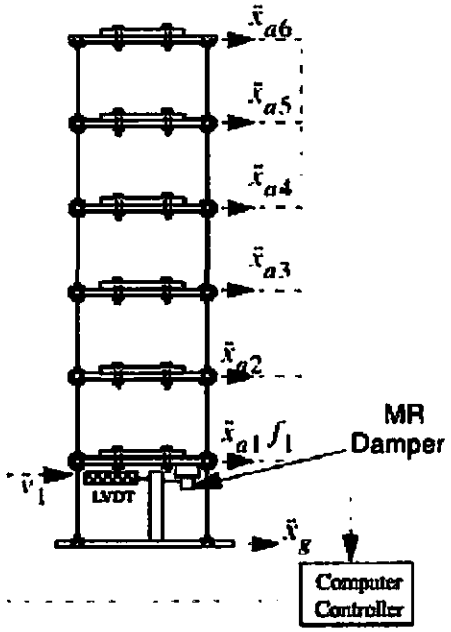

Fig. 4.36 Schematic view of the six-story building model with one MR damper

As shown in Fig. 4.36 is a six-story building model, the frequencies of this lumped mass model are 1.39, 4.08, 6.54, 8.62, 10.19 and 11.18 Hz, respectively.

In a similar way, we can plot the ratios of structural responses of the 1st floor versus a series of R, as shown in Figs 4.37-4.41.

- For relative displacement, generally the control efficiency under El-Centro earthquake is around 30%-90%. The ratios almost keep constant when R is within the range of $10^{-10} \sim 10^{-2}$. Then the control efficiency decreases sharply when R exceeds 10^{-2}. Such a sudden decrease appears more evident than that for stiff one-story building.
- In this case, MR damper achieve considerable reduction in displacement when the building undergo small, however, it also results in a larger acceleration.

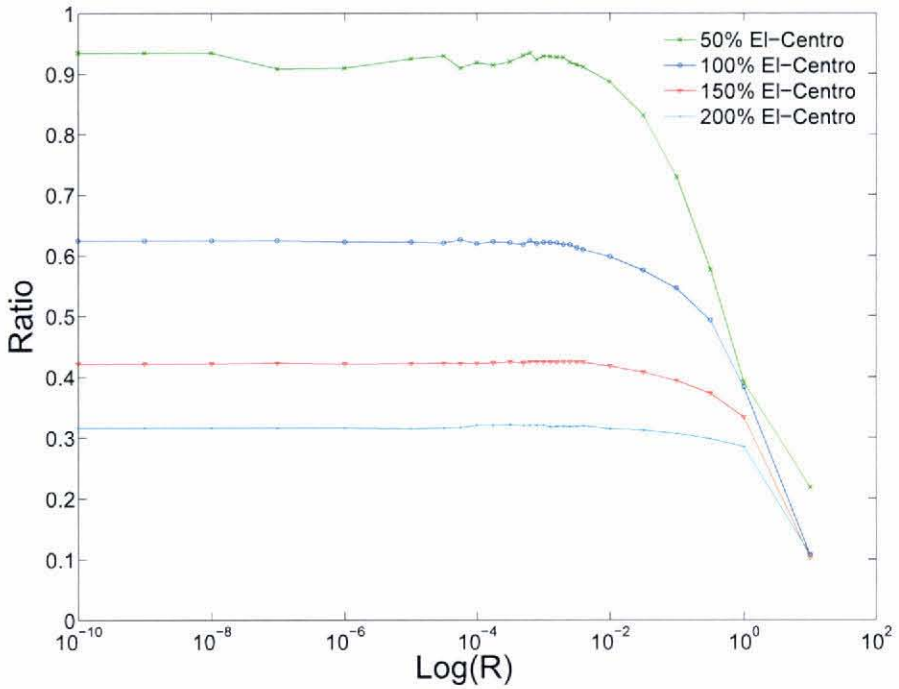

Fig. 4.37 Peak displacement of the 1st floor of six-story building excited by different amplitudes of El-Centro earthquake

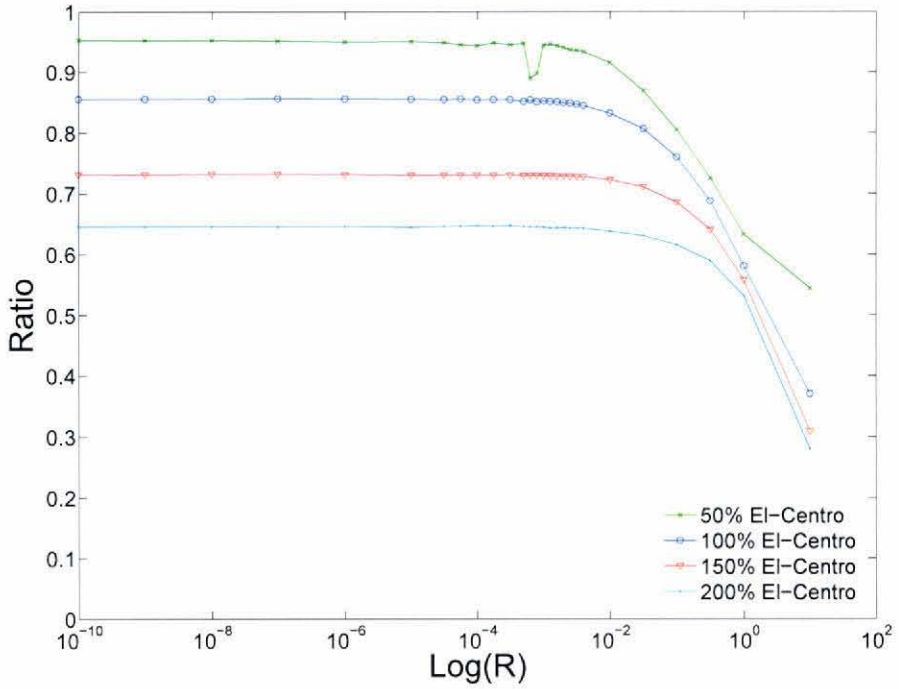

Fig. 4.38 RMS displacement of the 1st floor of six-story building excited by different amplitudes of El-Centro earthquake

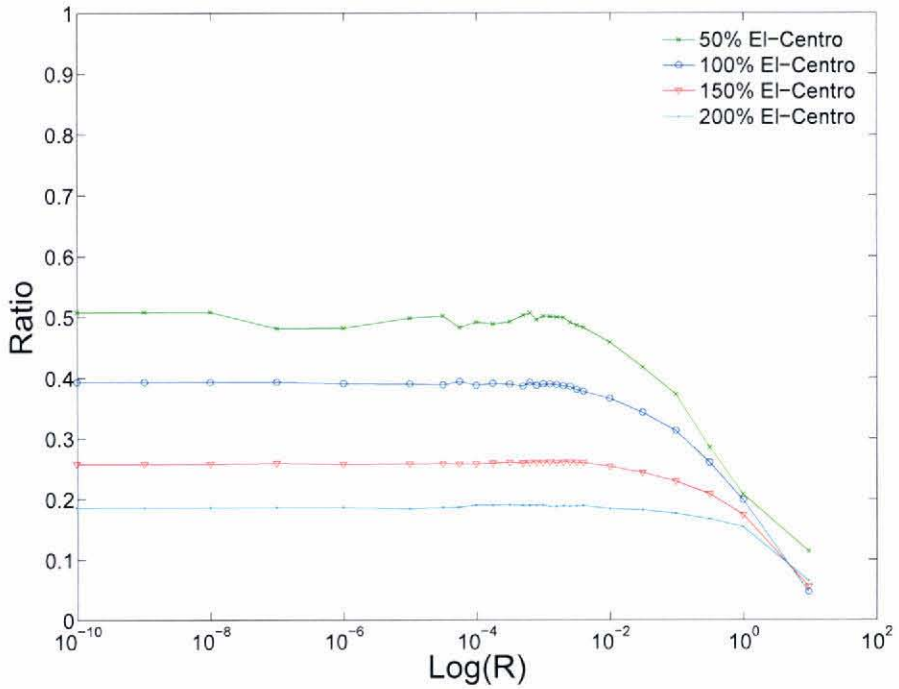

Fig. 4.39 Peak acceleration of the 1st floor of six-story building excited by different amplitudes of El-Centro earthquake

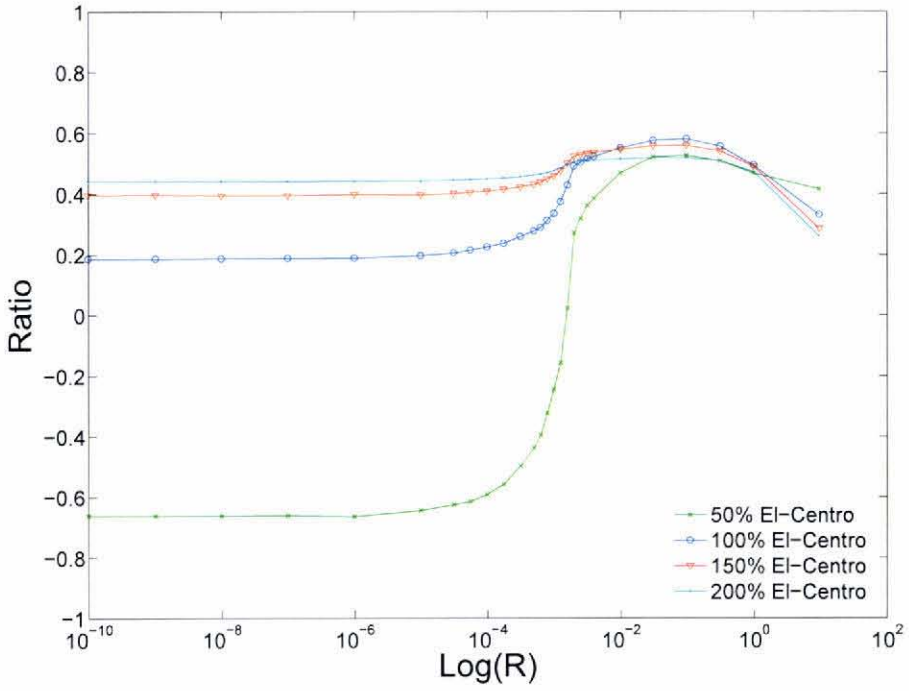

Fig. 4.40 RMS acceleration of the 1st floor of six-story building excited by different amplitudes of El-Centro earthquake

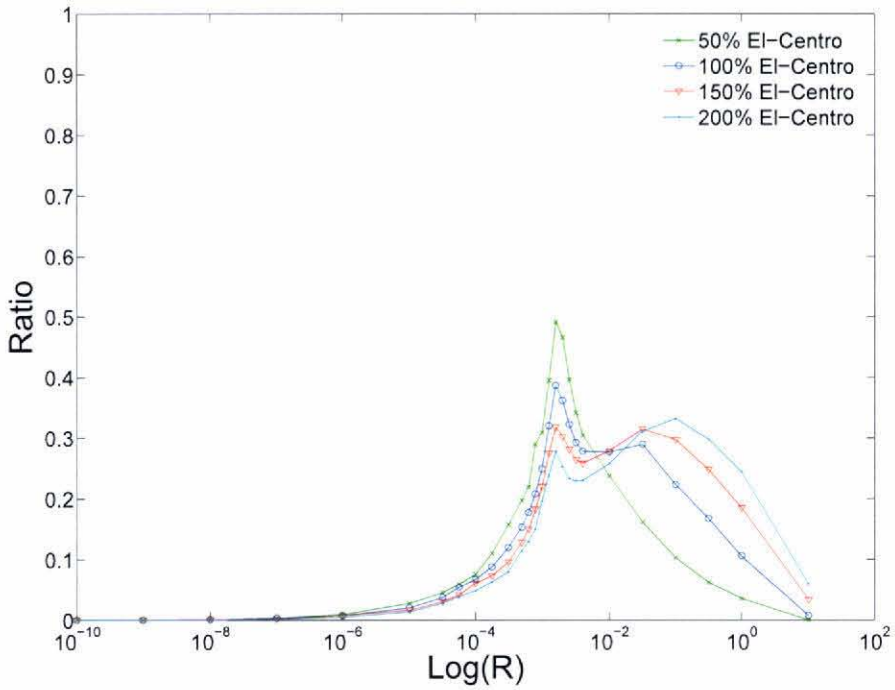

Fig. 4.41 Percentage of voltages between minimum and maximum for the 1st floor of six-story building excited by different amplitudes of El-Centro earthquake

4.4 Introduction of Program

As shown in the flowchart - Fig. 4.42, the objective is to calculate the structural response under scaled excitations and within a range of R.

START: To begin the main program.

INPUT: Input the properties of the building/MR damper, types of excitation, the number of scaled excitation (INDEX_SCALE) and values of R (INDEX_R).

CONTROL: This is the core module for each combination of (Q, R), in which the new control strategy is integrated with the *ode45* solver to solve the nonlinear equations. The details of this module are shown in Fig.4.43.

PROCESSING: Data from the controlled case are compared with those from

uncontrolled case, passive-on and passive-off cases.

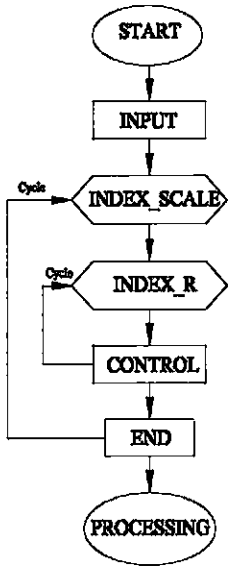

Fig. 4.42 Flowchart for program

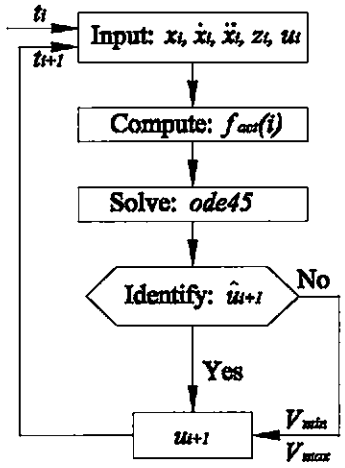

Fig. 4.43 Flowchart for module "CONTROL"

CHAPTER 5 Conclusions and Future Work

5.1 Conclusions

A semi-active control strategy is developed to command the MR damper an appropriate voltage by tracking the desired/optimal control force. In this strategy, a modified dynamic model for MR damper is successfully applied to estimate the evolutionary variable.

- It is validated that this new strategy can be applied to effectively reduce the structural response under various excitations.
- The MR damper can achieve the desired force well corresponding to an appropriate R . It can even achieve more efficient vibration control, when compared with the ideal case, in these examples.
- A better control can be achieved at passive-on case than at passive-off case when the excitation is moderate or strong, except for small amplitude excitation, as is consistent with the results presented by Janson and Dyke (2000).
- MR damper can perform a better control of all considered responses when R is around $10^{-2.5}$ - $10^{-1.5}$, corresponding the maximum percentage of intermediate voltages. Therefore, recommend to choose R around 10^{-2}.
- MR damper's performance is always limited by its capability, thus the corresponding control efficiency keeps almost stable.

5.2 Future Work

- The direct method presents a precise way to calculate the evolutionary variable. This advantage can be utilized to command the voltage to MR damper.
- Further research is needed to compare structural control of the same building excited by different earthquakes, using MR dampers. Guideline needs to be established and verified to command MR dampers when undergoing different kinds of earthquake.
- For multi-story building, two or more dampers can be placed in different stories. This will be helpful for us to understand how the dampers cooperate to resist the vibration.
- The effectiveness of this new control strategy needs to be verified in the lab test.

REFERENCE

Agrawal, A.K., Yang, J.N. and He, W.L. (2003) "Applications of some semi-active control systems to benchmark cable-stayed bridge", Journal of Structural Engineering, 129(7): 884-894.

Ahlawat, A.S. and Ramaswamy, A. (2001) "Multiobjective optimal structural vibration control using fuzzy logic control system", Journal of Structural Engineering, 127(11): 1330-1336.

Battaine, M., Casciati F. and Faravelli, L. (1998) "Fuzzy control of structural vibration: an active mass system driven by a fuzzy controller", Earthquake Engineering and Structural Dynamics, 27:1267-1276.

Chang, C.C. and Zhou, L. (2002) "Neural network emulation of inverse dynamics for a magnetorheological damper", Journal of Structural Engineering, 128(2): 231-239.

Chu, S.Y., Song, T.T. and Reinhorn, A.M. (1990) Active, hybrid, and semi-active structural control John Wiley & Sons, West Sussex, England.

Dyke, S.J., Caicedo, J.M., Turan, G, Bergman, L.A. and Hague, S. (2003) "Phase • • benchmark control problems for seismic response of cable-stayed bridges", Journal of Structural Engineering, 129(7): 857-871.

Ehrgott, R.C., Masri, S.F. 1992. "Modeling the oscillatory dynamic behavior of electrorheological materisals in shear ", Smart Materials Struct. 1,275-285.

Goncalves, F.D., Koo, J.H. and Ahmadian, M. (2006) "A review of the state of the art in magnetorheological fluid technologies- part • : MR fluid and MR fluid models", The Schock and Vibration Digest, 38(3): 203-219.

He, W.L., Agrawal, A.K. and Yang, J.N. and (2003). "Novel semiactive friction controller for linear structures against earthquakes", Journal of Structural Engineering, 129(7): 941-949.

Jolly, M.R., Bender, J.W. and Carlson, J.D. (1999). "Properties and applications of commercial magnetorheological fluids", Journal of Intelligent Material Systems and Structures, 10: 5-13.

Kamath, G.M. and Wereley, N.M. (1997) "A nonlinear visoelastic-plastic model for electrorheological fluids", Smart Materials Structures, 6: 351-359.

Kim, H.S. and Roschke, P.N. (2006) "Design of fuzzy logic controller for smart base isolation system using genetic algorithm", Engineering Structures, 28:84-96

Kim, H.S., Roschke, P.N., Lin, P.Y. and Loh, C.H. (2006) "Neuro-fuzzy model of hybrid semiactive base isolation system with FPS bearing and an MR damper", Engineering Structures, TBD:1-11

Kobori, T., Takahashi, M., Nasu, T., Niwa, N., and Ogasawara, K. (1993) "Seismic response controlled structure with active variable stiffness system", Earthquake Engineering and Structural Dynamics, 22:925-941.

Lee, T. and Kawashima, K. (2007) "Semiactive control of nonlinear isolated bridges with time delay", Journal of Structural Engineering, 133(2): 235-241.

Lewis, F.L. (1986) Optimal control, John Wiley & Sons, New York, pp. 180-193.

Lin, P.Y., Roschke, P.N. and Loh, C.H. (2006) "Hybrid base-Isolation with magnetorheological damper and fuzzy control", Structural Control and Health Monitoring, 13: 1-22.

Loh, C.H., Wu, L.Y. and Lin, P.Y. (2003) "Displacement control of isolated structures with semi-active control devices ", Journal of Structural Control, 10: 77-100.

Loh, C.H., Lynch, J.P et al. (2007) "Experimental verification of a wireless sensing and control system for structural control using MR dampers", Earthquake Engineering and Structural Dynamics, 36:1303-1328.

Lou, J.Y.K., Lutes, L.D and Li, J.J. (1994) "Active tuned liquid dampers for structural control", Proceedings of 1st world conferences on structural control, TP1: 70-79

Lynch, J.P., Wang, Y. et al. (2007) "Implementation of a closed-Loop structural control system using wireless sensor networks", Structural Control and Health Monitoring (in Press).

Makris, N., Burton, S.A. and Taylor, D.P. (1996) "Electrorheological damper with annular ducts for seismic protection applications ", Smart Materials Structures, 5: 551-564.

Nagarajaiah, S. and Narasimhan, S. (2007). "Seismic control of smart base isolated buildings with new semi-active variable damper", Earthquake Engineering and Structural Dynamics, 36, 729-749.

Ohtori, Y., Spencer, B.F. Jr, and Dyke, S.J. (2004) "Benchmark control problems for seismically excited nonlinear buildings", Jounal of Engineering Mechanics, 130(4): 366-385.

Patten, W.N. and Sack, R.L. (1996) "Controlled semiactive hydraulic vibration absorber for bridges", Journal of Structural Engineering, 122(2): 187-192.

Sadek, F. and Mohraz, B. (1998) "Semiactive control algorithms for structures with variable dampers", Journal of Engineering Mechanics, 124(9): 981-989.

Sahasrabudhe, S. and Nagarajaiah, S. (2005) "Effective of variable stiffness systems in base-isolated bridges subjected to near-fault earthquakes: an experimental and analytical study", Journal of Intelligent Material Systems and Structures, 16: 743-756.

Schurter, K., and Roschke, P. N., "Fuzzy modeling of a magnetorheological damper using ANFIS," Proceedings of the IEEE Fuzzy 2000 Conference, San Antonio, Texas, May, 2000.

Shen, Y., Golnaraghi, M.F. and Heppler, G.R. (2006) "Semiactive vibration control schemes for suspension systems using magnetorheological dampers", Journal of Vibration and Control, 12(1): 3-24

Song, J. and Kiureghian, A.D. (2006) "Generalized Bouc-Wen model for highly asymmetric hysteresis", Journal of Engineering Mechanics, 132(6): 610-618.

Song, X. (2007) "Decomposition approach to model smart suspension struts", Communcations in nonlinear science and numerical simulation, doi:10.1016/j.cnsns.2007.03.021.

Song, X., Ahmadian, M., Southward, S. and Miller L.R. (2005) "An adaptive semiactive control algorithm for magnetorheological suspension systems", Journal of Vibration and Acoustics, 127: 493-502.

Song, X., Ahmadian, M. and Southward, S. (2007) "Analysis and strategy for superharmonics with semiactive suspension control systems", Journal of Vibration and Acoustics, 129: 795-803.

Spencer, Jr., B.F., Suhardjo, J. and Sain, M. K. (1994). "Frequency domain optimal control strategies for aseismic protection", Journal of Engineering Mechanics, 120(1): 135-158.

Spencer, Jr., B.F., Dyke, S.J., et al. (1997) "Phenomenological model for magnetorheological dampers", Journal of Engineering Mechanics, 123(3): 230-238.

Spencer, Jr. B.F., and Nagarajaiah S. (2003) "State of the art of structural control", Journal of Structural Engineering, 129(7): 845-856.

Srinivasan, A.V. and McFarland, D.M. (2001) Smart structures – analysis and design, Cambridge University Press, Cambridge, UK, pp. 73-93.

Tsang, H.H., Su, R.K.K. and Chandler, A.M. (2006) "Simplified inverse dynamics models for MR fluid dampers." Engineering Structures, 28: 327-341.

Wang, C.H. and Chang, S.Y. (2007) "Development and validation of a generalized

biaxial hysteresis model", Journal of Engineering Mechanics, 133(2): 141-152.

Wang, D.H. and Liao, W.H. (2005) "Semiactive controller for magnetorheological fluid dampers", Journal of Intelligent Material Systems and Structures, 16: 983-993.

Wang, L.X. and Willatzen, M. (2007) "Nonlinear dynamical model for hysteresis based on nonconvex potential energy", Journal of Engineering Mechanics, 133(5): 506-513.

Wibgorasert, N. and Symans, M.D. (2005) "Experimental evalutation of adaptive elastomeric base-isolated structures using variable-orifice fluid dampers", Journal of Engineering Mechanics, 131(5): 867-877.

Yalla, S., Kareem, A. and Kantor, C. (2001) "Semiactive tuned liquid dampers for vibration control of structures", Engineering Structures, 23: 1469-1479.

Yang, G., Spencer, B.F., Carlson, J.D., and Sain, M.K. (2002) " Large-scale MR fluid dampers: modeling and dynamic performance considerations", Engineering Structures, 24: 309-323.

Yang, G., Spencer, B.F., Jung, H.J., and Carlson, J.D. (2004) " Large-scale MR fluid dampers: modeling and dynamic performance considerations", Journal of Engineering Mechanics, 130(9): 1107-1114.

Yang, J.N., Li, Z. and Vongchavalitkul, S. (1994) "Generalization of optimal control theory: Linear and nonlinear control", Journal of Engineering Mechanics, 120(2): 266-283.

Yang, J.N., Wu, J.C., Kawashima, K. and Unjoh, S. (1995) "Hybrid control of seismic excited bridge structures", Earthquake Engineering and Structural Dynamics, 24(11): 1437-1451.

Yang, J.N., Wu, J.C. and Li.Z. (1996) "Control of seismic-excited buildings using active variable stiffness systems", Engineering Structures, 18(8): 589-596.

Yoshida, O. and Dyke, S.J. (2004) "Seismic control of a nonlinear benchmark building using smart dampers", Journal of Engineering Mechanics, 130(4): 386-392.

Yoshida, O., Dyke, S.J., Giacosa, L.M. and Truman, K.Z. (2003) "Experimental verification on torsional response control asymmetric building using MR dampers", Earthquake Engineering and Structural Dynamics, 32: 2085-2105.

Zhou, L., Chang, C.C. and Wang, L.X. (2003) "Adaptive fuzzy control for nonlinear building-magnetorheological damper system", Journal of Structural Engineering, 129(7):905-913.

APPENDIX

A. Main program

```
%%%%%%%%%%%%%%%%%%%%%%%%%%%%%%%%%%%%%%%%%%%%%%%%%%%%%%%%%%%%%%%%%%%%%%%%%%%%%%%%%%%%%%%%%%%%%%%%%%%%%%%%%%%
%
% File name: Main.m.
% Main program of seismic control of multi-story buildings using one MR damper
at
% the 1st floor.
% Here are two choices: 1-story building and 6-story building.
% LQR method used here.
%
%%%%%%%%%%%%%%%%%%%%%%%%%%%%%%%%%%%%%%%%%%%%%%%%%%%%%%%%%%%%%%%%%%%%%%%%%%%%%%%%%%%%%%%%%%%%%%%%%%%%%%%%%%%

%--- INPUT STARTS---%
% Definition of the building
N=1;                % Dimension of the building: 1 or 6
m=0.227;             % 22.7 Kg= 0.227 N/cm/s2
k=297;              % 297 N/cm
zeta=0.01;           % N-sec/cm

% Bouc-Wen model for MR damper
C0a=0.032; C0b=0.02; alpha_a=27.3; alpha_b=26.5; gamma=300; beta=300;
A=120;Vmax=4.0;Vmin=0.0;

% Choose excitation type and its scale.
quake=3;                %1= El-centro earthquake; 2= Kobe; 3=WGN1
scale(:,1)=[0.5;1.0;2.0;5.0;10.0];   % scale(:,1)=[2.00;5.00];%

% Chose the control method (LQR method).
Q=1*diag(ones(1,2*N));
for i=1:1:9
  Rlqr(i,1)=10^(-10)*10^(0.5*(i-1))
end
for i=10:1:17
  Rlqr(i,1)=10^(-6)*10^(0.25*(i-9))
end
for i=18:1:47
  Rlqr(i,1)=10^(-4)*10^(0.1*(i-17))
end
for i=48:1:55
  Rlqr(i,1)=10^(-1)*10^(0.25*(i-47))
```

```
end
%--- INPUT ENDS---%

%--- PRELIMNARY PROCEDURES FOR MAIN PROGRAM (START)---%
% Defintions of m, c, k and other properties of buildings
mck=[m zeta k];
if N==1
   w=sqrt(k/m);
end
if N==6
   w=[1.39 4.08 6.54 8.62 10.19 11.18]*2*pi;
   w=diag(w);
end

% Bouc-Wen model for MR damper
Zu=A/(gamma+beta);

% Choose earthquake
if  quake==1
load elcentro.mat;
  ts_ini=elcentro(1,:);
    ddX0_ini=elcentro(2,:);
end
if quake==2
      load kobeew.mat;
      ts_ini=kobeew(:,1);
   ddX0_ini=kobeew(:,2);
end
if quake==3
   load filtered_wgn1.mat
   ts_ini=filtered_wgn1(:,1);
   ddX0_ini=filtered_wgn1(:,2);
end

% Define the time span of earthquake
% For earthquake
if quake==1 | quake==2
for j=1:1:(2*length(ts_ini)-1)
   s(j)=(j-1)*0.01;
      if mod(j,2)==0
         ddX0(j)=ddX0_ini(j/2);
      else
         ddX0(j)=ddX0_ini((j+1)/2);
      end
```

```
end
end

% For filtered-white-gaussian noise:
if quake==3
for j=1:1:(length(ts_ini))
   s(j)=(j)*0.01;
      ddX0(j)=ddX0_ini(j);
end
end

% Time length of excitation
ne=length(ts);
for j=1:1:ne
    ddX0_unit(j)=100*ddX0(j);  % Transform the unit from m/s^2 to cm/s^2;
end

% Construct matrices M, C, K
M=diag(ones(1,N));
K=diag(-ones(1,N-1),1)+diag(-ones(1,N-1),-1)+2*diag(ones(1,N))-diag([zeros(1,N-1)
1]);
M=m*M;Cn=2*zeta*M*w; K=k*K;
iM=inv(M);

% Calculate the eigenvalues and eigenvecor
[V,D]=eig(iM*K);Mn=V'*M*V;Kn=V'*K*V;
c=(Mn*V*iM)*Cn*(iM*V'*Mn);

F11=zeros(N,N); F12=diag([ones(1,N)]);          % Matrix A, 1st row
F21=-iM*Kn;     F22=-iM*c;                % Matrix A, 2nd row
A0=[F11 F12;F21 F22];

B2_1st=[zeros(N,1);iM(1,1)*1;zeros(N-1,1)];          %Number and position of
dampers
B1=[zeros(N,1);ones(N,1)];B2=[B2_1st];
%-- PRELIMNARY PROCEDURES FOR MAIN PROGRAM (END)---%

%%%%%%%%%%%%%%%%%%%%%%%%%%%%%%%%%%%%%%%%%%%%%%%%%%%%%%%%%%%%%%%%%%%%%%%%
%%%%%%%%%%
%
%            MAIN PROGRAM STARTS:
%
%%%%%%%%%%%%%%%%%%%%%%%%%%%%%%%%%%%%%%%%%%%%%%%%%%%%%%%%%%%%%%%%%%%%%%%%
%%%%%%%%%%
```

```
for index_scale=1:1:length(scale(:,1))   % For each sacled excitation, STARTS:

 % Scale the excitation:
      for j=1:1:ne
      ddX0(j)=scale(index_scale,1)*ddX0_unit(j);  % Transform the unit from m/s^2
to cm/s^2;
      end

%%%%%%%%%%----------------------------------------------------------------
%
%  For each scaled excitation, calculate the response at different (Q, R),
%
%%%%%%%%%%----------------------------------------------------------------

for index_R=1:1:length(Rlqr(:,1))

% Choose the control method
      R=Rlqr(index_R,1);
      G=lqr(A0,B2,Q,R);

% Initial state
      Z0=[zeros(2*N+1,1)];
      u(1)=0;

%Numerical calculation for R (index_R):

for i=1:ne-1

      fu_LQR(i)=-G*Z0(1:2*N,1);
      alpha(i,1)=alpha_a+alpha_b*u(i);C0(i,1)=C0a+C0b*u(i);
      fu_act(i)=-(C0(i,1)*Z0(N+1)+alpha(i,1)*Z0(2*N+1));
      acc(1:N,i)=F21*(Z0(1:N))+F22*(Z0((N+1):2*N))+[B2((N+1):2*N)]*fu_act(i);

% ODE45 starts,
   [t0 y0]=ode45('multi_bldg', [ts(i) ts(i+1)], Z0, [ ],[ts(i) ts(i+1) ddX0(i) N mck u(i)
fu_act(i)]);
   index=length(t0);
     if y0(index,2*N+1)>Zu
        y0(index,2*N+1)=Zu;
       else if y0(index,2*N+1)<-Zu
         y0(index,2*N+1)=-Zu;
     end
 end
```

```
% Judge the range of voltage
NUM=(-fu_LQR(i)-C0a*y0(index,N+1)-alpha_a*y0(index,2*N+1));
DENOM=(C0b*y0(index,N+1)+alpha_b*y0(index,2*N+1));
if DENOM==0.0
      u(i+1,1)=0.0;
else
      u(i+1,1)=NUM/DENOM;
end

if u(i+1,1)>Vmax
      u(i+1,1)=Vmax;
      else if u(i+1,1)<Vmin
                u(i+1,1)=Vmin;
      end
end
% Get the vector at t(i+1) and define the initial value at t(i+1)
    y_vector(i+1,1:(2*N+1))=y0(index,:);
    Z0=y0(index,:)';
end
%Numerical calculation ends!


%Derive the extreme values or RMS of structural responses for R(index_R):
data(index_R,1)=Rlqr(index_R,1);
data(index_R,2)=max(abs(y_vector(:,1)));
data(index_R,3)=max(abs(y_vector(:,2)));
data(index_R,4)=max(abs(acc(:)));
data(index_R,5)=norm(y_vector(:,1))/sqrt(length(y_vector(:,1)));
data(index_R,6)=norm(y_vector(:,2))/sqrt(length(y_vector(:,1)));
data(index_R,7)=norm(acc(:))/sqrt(length(acc(:)));

% Count the number of voltage between Min. and Max.
count=0;i=1;
for i=1:1:length(u)
      if u(i)<4.0 & u(i)>0.0
      count=count+1;
      else
      count=count;
      end
end
data(index_R,8)=count;

% Count the number of evolutionary variable Zu between Max. (=0.2) and Min. of zu
```

```
count2=0;i=1;
for i=1:1:length(y_vector(:,3))
     if y_vector(i,3)<0.2 & y_vector(i,3)>0.0
    count2=count2+1;
     else
    count2=count2;
     end
end
data(index_R,9)=count2;

% Count the number of evolutionary variable Zu between Max. (=0.199) and Min. zu;.
count3=0;i=1;
for i=1:1:length(y_vector(:,3))
     if y_vector(i,3)<0.199 & y_vector(i,3)>0.0
    count3=count3+1;
     else
    count3=count3;
     end
end
data(index_R,10)=count3;
end                 % R(index_R) ENDS!

%%%%%%%%%%----------------------------------------------------------------
%
%  For each scaled excitation, calculate the response at different (Q, R),
%  ENDS!
%%%%%%%%%%----------------------------------------------------------------

results(index_scale).scale=scale(index_scale,1);  % Record the # of scale for each
scaled excitation.
results(index_scale).data(:,:)=data(:,:);        % Results due to xx times scaled
excitation.
end                              % For each sacled excitation, ENDS!

%%%%%%%%%%%%%%%%%%%%%%%%%%%%%%%%%%%%%%%%%%%%%%%%%%%%%%%%%%%%%%%%%%%%%%%%%%%%
%
%            MAIN PROGRAM ENDS!
%
%%%%%%%%%%%%%%%%%%%%%%%%%%%%%%%%%%%%%%%%%%%%%%%%%%%%%%%%%%%%%%%%%%%%%%%%%%%%
```

B. Sub-function

```
%%%%%%%%%%%%%%%%%%%%%%%%%%%%%%%%%%%%%%%%%%%%%%%%%%%%%
%%%%%%%%%%%%%%%
%   File name: 'Multi_bldg.m'  (Subfuction of 'Main.m')
%   Use only one MR damper at the 1st floor of multi-story building.
%   LQR method is adopted here.
%%%%%%%%%%%%%%%%%%%%%%%%%%%%%%%%%%%%%%%%%%%%%%%%%%%%%
%%%%%%%%%%%%%%%

function dydt=multi_bldg(t,y0,init,paras)
% Parameters:
ddX0i=paras(3);N=paras(4);   m=paras(5);  zeta=paras(6); k=paras(7);u=paras(8);
fu=paras(9);
gamma=300; beta=300;A_damp=120;

% Define the vector "dydt"
dydt=zeros(2*N+1,1);
if N==1
     w=sqrt(k/m);
end
if N==6
     w=[1.39 4.08 6.54 8.62 10.19 11.18]*2*pi;w=diag(w);
end

%Construct parameter matrices M, C, K
M=diag(ones(1,N));
K=diag(-ones(1,N-1),1)+diag(-ones(1,N-1),-1)+2*diag(ones(1,N))-diag([zeros(1,N-1)
1]);
M=m*M; Cn=2*zeta*M*w; K=k*K;
iM=inv(M);                              % Inverse the Mass matrix M

%Calculate the eigenvalues and eigenvector
[V,D]=eig(iM*K);
Mn=V'*M*V;Kn=V'*K*V;
c=(Mn*V*iM)*Cn*(iM*V'*Mn);

%Initial states
x=y0(1:N);dx=y0(N+1:2*N);z=y0(2*N+1);

%Calculate matrix A, B & W
F11=zeros(N,N); F12=diag([ones(1,N)]);              % Matrix A, 1st row
F21=-iM*Kn;     F22=-iM*c;                    % Matrix A, 2nd row
A=[F11 F12;F21 F22];
```

```
B2_1st=[zeros(N,1);iM(1,1)*1;zeros(N-1,1)];
B1=[zeros(N,1);ones(N,1)];                    % Coefficient for earthquake
B2=[B2_1st];                                  % Coefficient for control  force, 2Nx1

%States output
dydt(1:(2*N),1)=A*[x; dx]+B2*fu-B1*ddX0i*1.0;
dydt((2*N+1),1)=-gamma*abs(y0(N+1,1))*z-
beta*y0(N+1,1)*abs(z)+A_damp*y0(N+1,1);
end
```